Hydro-mechanical fracture modeling governed by topological derivatives

M. Xavier[a], N. Van Goethem[c,*], A.A. Novotny[b]

[a] *Universidade Federal Fluminense UFF, TEM - Departamento de Engenharia Mecânica, Rua passo da Pátria 156, 24210-240 Niterói - RJ, Brazil*
[b] *Laboratório Nacional de Computação Científica LNCC/MCTIC, Coordenação de Matemática Aplicada e Computacional, Av. Getúlio Vargas 333, 25651-075 Petrópolis - RJ, Brazil*
[c] *Universidade de Lisboa, Faculdade de Ciências, Departamento de Matemática, CMAFcIO, Alameda da Universidade, 1749-016 Lisboa, Portugal*

Abstract

The process of fluid-driven crack propagation in permeable rocks is investigated by a simple hydro-mechanical model and the concept of topological derivative. Analytical and numerical computations are made to propose a promising model tested and validated on a series of bidimensional benchmark examples. The main guidelines for this model are the use of simple finite elements with a minimal number of user-defined algorithmic parameters.
© 2020 Elsevier B.V. All rights reserved.

1. Introduction

The hydraulic fracturing process is an engineering technique used to create and/or propagate geological faults by means of the pressure of an injected fluid in order to let the gas trapped inside the rock be extracted at the surface. This extraction process, commonly known as *fracking*, can be extremely damageable for the ecosystem due, in part, to the possibility of contamination of the soil and the creation of uncontrolled seismic effects provoked by the initiation and propagation of the cracks. In this sense, it is essential to promote accurate developments of theoretical studies as well as computational tools able to monitor and possibly optimize the real-world process. This simulation-based approach eventually serves as a scientific support at the disposal of the decision and policy makers.

The hydraulic fracturing process has been subject of intense research in last years, see for example [1–8], to cite a few. For a comprehensive review on the subject, see the introduction section in [9], where a phase-field approximation in the spirit of Francfort–Marigo variational approach [10,11] is proposed. See also [12] where the full Biot system is combined with a phase-field approach for hydraulic fracture modeling in a porous medium. A fully-coupled formulation accounting for the displacement, pressure and the phase-field itself has been proposed in [13], based on a free energy functional governing the whole damage evolution process.

---

* Corresponding author.
E-mail addresses: marcelxavier@id.uff.br (M. Xavier), vangoeth@fc.ul.pt (N. Van Goethem), novotny@lncc.br (A.A. Novotny).

Recently, a simplified hydraulic fracturing model also based on the minimization of the Francfort–Marigo functional but using the concept of topological derivative [14–18] to nucleate and propagate the cracks has been introduced in [19]. Both approaches of [9] and [19] are similar in spirit in the sense that on the one hand they are damage or "smeared crack" approaches to fracture (that is, by means of an infinitesimal parameter), and on the other hand they avoid the introduction of ad-hoc tools, such as geometry or crack dependent parameters. Moreover, both are based on an unified method to compute the crack opening and the mechanical equilibrium, possibly coupled, as in the present work, to a porous media model, computed on the same domain discretization. We stress however that in our method, the main guideline is the minimal working assumptions, parameters, and equations into play. We also emphasize that nucleation and propagation are both governed by a threshold approach for the topological derivative field, leading to remarkably simple algorithm that features a minimal number of user-defined algorithmic parameters.

In the proposed methodology of [19], the reservoir was modeled as a two dimensional idealization in which the rock is assumed to be impermeable and with no porosity. In this particular case, the fluid pressure is constant and confined inside the crack. Obviously, this is not what takes place in the real process of hydraulic fracture, because the reservoir generally consists in a porous medium. Therefore, the proposed pressure evolution strategy was in this preliminary work a severe simplification of the fracking process encountered in real world, but nonetheless the methodology we have followed seemed promising, allowing for the detection of multiples crack tip opening and the simultaneous computation of multiple fracture paths. Moreover, the obtained results showed typical features of hydraulic fracture, such as the characterization of the fault-activation pressure and specific crack path growth, allowing for kinking and bifurcations. Also, the theoretical study motivated by the fracking model, made in [20] and consisting in a Γ-convergence result of the damage to the sharp fracture model, was a further preliminary step to the understanding and the improvement of our model.

Indeed, in the present work, we propose an improvement of the method by letting the propagating medium be permeable and hence we extend the strategy introduced in [19] for a porous media taking into account the hydro-mechanical model proposed by Biot [21]. In this case, the crack propagation mechanism is activated by non constant pressure field distributed over the whole domain. The resulting model is semi-coupled in the sense that the equation for the displacement depends on the pressure through a source term, whereas the equation for the pressure has no dependence on the displacement, and thus is unable to account for the influence of the fluid on the porous matrix. Therefore, in contrast to our former work [19], a much more realistic scenario which takes into account for pressure dropping phenomenon within the crack is considered. In addition, a specific adjoint state is introduced in order to derive the associated sensitivities, that is solution to a semi-coupled problem in a reverse sense, where the adjoint pressure system depends on the displacement field. This extension is non-trivial and represents the main contribution of the paper from both theoretical and practical point of views. It should be emphasized, however, that we are interested in the analysis of one particular aspect of the hydraulic fracturing process, namely, the effect of a non constant distributed pressure field on the mechanism of crack propagation inside a porous medium. In this sense, we stress that several physical aspects associated with the real hydraulic fracturing process, such as thermal and chemicals effects or elastic waves produced by explosives, are yet neglected. The treatment of the total coupled case, in transient regime into three spatial dimensions, is now under investigation.

The work is organized as follows. The hydro-mechanical model of hydraulic fracture is introduced in Section 2. In Section 3, the associated topological derivative expression is derived. The topology optimization algorithm is presented in Section 4. The numerical experiments are shown in Section 5. The theoretical results in three spatial dimensions are presented in Section 6 for the reader convenience. Finally, some concluding remarks are presented in Section 7.

2. Hydro-mechanical model of hydraulic fracture

Let us consider a saturated porous matrix submitted to a fluid flux that obeys the Darcy law under the quasi-static loading assumption. The porous matrix, which represents a single block of the reservoir, is given by an open and bounded geometric domain $\Omega \subset \mathbb{R}^2$ with Lipschitz boundary $\partial\Omega$. The domain Ω contains a subdomain $\omega \subset \Omega$, representing the geological fault into the reservoir. See Fig. 1. In the proposed model ω is a damage region, and it is only in the limit that this damage model is a fracture model, see [20]. To characterize the damage region, a parameter ρ, defined as

$$\rho = \rho(x) := \begin{cases} 1, & \text{if } x \in \Omega \setminus \overline{\omega}, \\ \rho_0, & \text{if } x \in \omega, \end{cases} \tag{2.1}$$
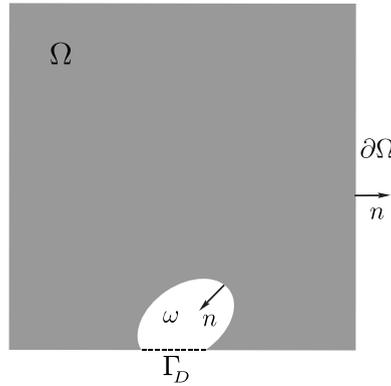
Fig. 1. Saturated block containing a geological fault.

with $0 < \rho_0 \ll 1$, is introduced. Then, the region $\Omega \setminus \overline{\omega}$ will represent the undamaged porous medium while ω the geological fault. Since the present model is derived from the one proposed by Francfort–Marigo [10,11], the idea consists in minimizing a shape functional $\mathcal{F}_\omega(u)$ of the form

$$\mathcal{F}_\omega(u) = \mathcal{J}(u) + \kappa |\omega| , \tag{2.2}$$

with respect to the geological fault ω, at the quasi-static time step t_i. The second term on the right hand side of (2.2) is the Griffith's energetic dissipation term while $\mathcal{J}(u)$ represents the total potential energy of the system and is written as

$$\mathcal{J}(u) = \frac{1}{2} \int_\Omega \sigma(u) \cdot (\nabla u)^s \, dx - \int_\Omega \alpha \, p \, \mathrm{div}(u) \, dx . \tag{2.3}$$

The displacement field u, at the quasi-static time step t_i, is solution to the following variational problem: Find $u \in \mathcal{U}$, such that

$$\int_\Omega \sigma(u) \cdot (\nabla \eta)^s \, dx = \int_\Omega \alpha \, p \, \mathrm{div}(\eta) \, dx , \quad \forall \eta \in \mathcal{V} , \tag{2.4}$$

where α is the Biot's coefficient [21] and p is the pressure of the fluid acting into the porous matrix at the time step t_i. More precisely, $p = p(x)$ is solution to the following variational problem: Find $p \in \mathcal{P}$ such that

$$\int_\Omega k \nabla p \cdot \nabla \varphi \, dx = 0 , \quad \forall \varphi \in \mathcal{Q} . \tag{2.5}$$

The term $\sigma(\varphi)$ in (2.3) represents the stress tensor and is defined as

$$\sigma(\varphi) = \rho \mathbb{C}(\nabla \varphi)^s , \tag{2.6}$$

with the parameter ρ given by (2.1). We consider that the reservoir is composed of an isotropic material, so that the elasticity tensor $\mathbb{C}$ can be written as follows

$$\mathbb{C} = 2\mu \mathbb{I} + \lambda (\mathrm{I} \otimes \mathrm{I}) , \tag{2.7}$$

where I and $\mathbb{I}$ are the second and fourth identity tensors, respectively, and μ and λ, given by

$$\mu = \frac{E}{2(1+\nu)} \quad \text{and} \quad \lambda = \frac{\nu E}{(1+\nu)(1-2\nu)} , \tag{2.8}$$

are the Lamé's coefficients. The strain tensor, denoted by $(\nabla \varphi)^s$, is defined as

$$(\nabla \varphi)^s := \frac{1}{2}(\nabla \varphi + (\nabla \varphi)^\top) . \tag{2.9}$$

The permeability of the porous medium k in (2.5) assume the values

$$k = k(x) := \begin{cases} k_r, & \text{if } x \in \Omega \setminus \overline{\omega} , \\ k_f, & \text{if } x \in \omega , \end{cases} \tag{2.10}$$

with $k_r \ll k_f$. The set $\mathcal{U}$ and the space $\mathcal{V}$ are defined as

$$\mathcal{V} := \mathcal{U} := H_0^1(\Omega; \mathbb{R}^2) , \tag{2.11}$$

while the set $\mathcal{P}$ and the space $\mathcal{Q}$ are given by

$$\mathcal{P} := \left\{ \varphi \in H^1(\Omega) : \varphi_{|\Gamma_0} = 0 , \ \varphi_{|\Gamma_D} = \overline{p}_i \right\} \text{ and } \mathcal{Q} := \left\{ \varphi \in H_0^1(\Omega) \right\} , \tag{2.12}$$

where $\Gamma_0 := \partial \Omega \setminus \Gamma_D$. The term $\overline{p}_i$ in the set $\mathcal{P}$ represents a prescribed pressure on Γ_D at the time step t_i, such that

$$\overline{p}_i = \overline{p}_{i-1} + \Delta \overline{p}_i , \tag{2.13}$$

where $\Delta \overline{p}_i$ represents the pressure increment. Then, the total prescribed pressure $\overline{p}$ is given by the sum

$$\overline{p} = \overline{p}_0 + \sum_{i=1}^{N} \Delta \overline{p}_i , \tag{2.14}$$

where $\overline{p}_0$ is the initial prescribed pressure and N the total number of increments. Therefore, the displacement field u and the pressure p, in each quasi-static time step t_i, are induced by the boundary condition $\overline{p}_i$ prescribed on Γ_D. Finally, the following adjoint problem is introduced in order to simplify future derivations: Find $q \in \mathcal{Q}$, such that

$$\int_{\Omega} k \nabla q \cdot \nabla \varphi \, dx = \int_{\Omega} \alpha \, \text{div}(u) \, \varphi \, dx , \ \forall \varphi \in \mathcal{Q} , \tag{2.15}$$

where α is the Biot's coefficient.

Taking into account all these elements, the minimization problem can be defined as: For each quasi-static time instant t_i,

$$\underset{\omega \subset \Omega}{\text{Minimize}} \ \mathcal{F}_\omega(u), \ \text{subject to (2.4)} , \tag{2.16}$$

where $\mathcal{F}_\omega(u)$ is given by (2.2).

The same strategy proposed in [19] to deal with the characterization of the critical pressure is adopted here, i.e., the parameter κ is replaced by a new parameter κ_δ defined as

$$\kappa = \kappa_\delta := \frac{\kappa_s}{\delta} , \tag{2.17}$$

where κ_s represents a new material property and δ is the length of the initial damage. The scaling property of κ with respect to δ is crucial in the proof of the Γ-convergence result in [20].

3. Topological derivative method

The topological derivative is defined as the first term of the asymptotic expansion of a given shape functional with respect to a small parameter that measures the size of singular domain perturbations, such as holes, inclusions, source-terms and cracks. In other words, the topological derivative measures the sensitivity of the associated shape functional with respect to the nucleation of a singular domain perturbation. In order to introduce these ideas, let us consider an open and bounded domain $\Omega \subset \mathbb{R}^2$ with a Lipschitz boundary $\partial \Omega$, which is subject to a nonsmooth perturbation confined in a small region $B_\varepsilon(\hat{x})$ of size ε centered at an arbitrary point $\hat{x} \in \Omega$. We introduce a characteristic function $x \mapsto \chi(x)$, $x \in \mathbb{R}^2$, associated with the unperturbed domain, namely $\chi = \mathbb{1}_\Omega$, such that:

$$|\Omega| = \int_{\mathbb{R}^2} \chi(x) dx , \tag{3.1}$$

where $|\Omega|$ is the Lebesgue's measure of Ω. Then, we define a characteristic function associated with the topologically perturbed domain of the form $x \mapsto \chi_\varepsilon(\hat{x}; x)$, $x \in \mathbb{R}^2$. In the case of a perforation, for example, $\chi_\varepsilon(\hat{x}) = \mathbb{1}_\Omega - \mathbb{1}_{B_\varepsilon(\hat{x})}$, the perforated domain is obtained as $\Omega_\varepsilon(\hat{x}) = \Omega \setminus \overline{B_\varepsilon(\hat{x})}$. Finally, we assume that a given shape functional $\psi(\chi_\varepsilon(\hat{x}))$, associated with the topologically perturbed domain, admits the following topological asymptotic expansion:

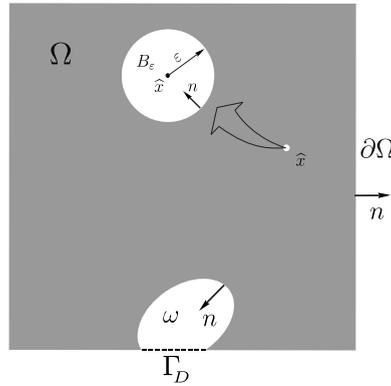$$\psi(\chi_\varepsilon(\hat{x})) = \psi(\chi) + f(\varepsilon) D_T \psi(\hat{x}) + o(f(\varepsilon)) , \tag{3.2}$$

Fig. 2. Perturbed problem.

where $\psi(\chi)$ is the shape functional associated to the original domain, that is, without perturbation, $f(\varepsilon)$ is a positive function such that $f(\varepsilon) \to 0$ when $\varepsilon \to 0$ and $o(f(\varepsilon))$ is the remainder. The function $\hat{x} \mapsto D_T \psi(\hat{x})$ is called the topological derivative of ψ at $\hat{x}$, which can be used as a steepest-descent direction in an optimization process like in any method based on the gradient of the cost functional.

Therefore, in order to evaluate the topological derivative of the shape functional (2.2), it is necessary first to introduce the topologically perturbed problem. The idea consists in nucleate a small circular inclusion, denoted by $B_\varepsilon(\hat{x})$, of radius ε and centered at the point $\hat{x} \in \Omega$, such that $\overline{B_\varepsilon(\hat{x})} \subset \Omega$ and $\overline{B_\varepsilon(\hat{x})} \cap \partial\omega = \emptyset$ (see Fig. 2). The hydro-mechanical properties at the inclusion $B_\varepsilon(\hat{x})$ will be the same as in the geological fault ω. In order to introduce the topological perturbation, let us consider three piece-wise constant functions, γ_ε, $\gamma_\varepsilon^\alpha$ and γ_ε^f, which are defined as

$$\gamma_\varepsilon = \gamma_\varepsilon(x) := \begin{cases} 1 & \text{if } x \in \Omega \setminus \overline{B_\varepsilon} , \\ \gamma & \text{if } x \in B_\varepsilon , \end{cases} \tag{3.3}$$

$$\gamma_\varepsilon^\alpha = \gamma_\varepsilon^\alpha(x) := \begin{cases} 1 & \text{if } x \in \Omega \setminus \overline{B_\varepsilon} , \\ \gamma^\alpha & \text{if } x \in B_\varepsilon , \end{cases} \tag{3.4}$$

and

$$\gamma_\varepsilon^f = \gamma_\varepsilon^f(x) := \begin{cases} 1 & \text{if } x \in \Omega \setminus \overline{B_\varepsilon} , \\ \gamma^f & \text{if } x \in B_\varepsilon , \end{cases} \tag{3.5}$$

that affect the elasticity tensor $\mathbb{C}$, the Biot's coefficient α and the permeability k, respectively, as described in detail in Sections 3.1 and 3.2. The shape functional associated with the topological perturbed problem is written as

$$\mathcal{F}_{\omega_\varepsilon}(u_\varepsilon) = \mathcal{J}_\varepsilon(u_\varepsilon) + \kappa |\omega_\varepsilon| , \tag{3.6}$$

where $\omega_\varepsilon = \omega \cup B_\varepsilon$ with $\omega \cap B_\varepsilon = \emptyset$ and $\mathcal{J}_\varepsilon(u_\varepsilon)$ denotes the total potential energy of the perturbed system.

Since the present problem is formulated under a linear regime, the asymptotic analysis can be done separately. In Section 3.1, the perturbation is considered on the elastic properties (elasticity tensor) and on the Biot's coefficient by setting $\gamma^f = 1$, $\gamma \neq 1$ and $\gamma^\alpha \neq 1$. In Section 3.2, the analysis will be done with respect to a perturbation on the permeability by setting $\gamma = \gamma^\alpha = 1$ and $\gamma^f \neq 1$. The final result is summarized in Section 3.3.

3.1. Perturbation on the elastic properties and on the Biot's coefficient

As mentioned above, the topological asymptotic analysis will be done first with respect to the perturbation on the mechanical properties and on the Biot's coefficient, i.e., with $\gamma \neq 1$, $\gamma^\alpha \neq 1$ and $\gamma^f = 1$. In this case, the total potential energy associated with the perturbed system, denoted by $\mathcal{J}_\varepsilon(u_\varepsilon)$, is written as

$$\mathcal{J}_\varepsilon(u_\varepsilon) = \frac{1}{2} \int_\Omega \sigma_\varepsilon(u_\varepsilon) \cdot (\nabla u_\varepsilon)^s \, dx - \int_\Omega \alpha_\varepsilon p \, \text{div}(u_\varepsilon) \, dx , \tag{3.7}$$

where the vector function u_ε is solution to the following variational problem: Find $u_\varepsilon \in \mathcal{U}$, such that

$$\int_\Omega \sigma_\varepsilon(u_\varepsilon) \cdot (\nabla \eta)^s \, dx = \int_\Omega \alpha_\varepsilon \, p \operatorname{div}(\eta) \, dx \, , \quad \forall \eta \in \mathcal{V}, \tag{3.8}$$

with $\sigma_\varepsilon(u_\varepsilon) = \gamma_\varepsilon \sigma(u_\varepsilon)$ and $\alpha_\varepsilon = \gamma_\varepsilon^\alpha \alpha$, where $\sigma(\varphi)$, γ_ε and $\gamma_\varepsilon^\alpha$ are given by (2.6), (3.3) and (3.4), respectively, and α is the Biot's coefficient. In order to evaluate the difference between the energy shape functionals $\mathcal{J}(u)$ and $\mathcal{J}_\varepsilon(u_\varepsilon)$, defined in (2.3) and (3.7), respectively, let us take $\eta = u_\varepsilon - u$ as test function in the variational equation (2.4). Then, the following equality is obtained

$$\int_\Omega \sigma(u) \cdot (\nabla u)^s \, dx = \int_\Omega \sigma(u) \cdot (\nabla u_\varepsilon)^s \, dx - \int_\Omega \alpha \, p \operatorname{div}(u_\varepsilon - u) \, dx \, . \tag{3.9}$$

Replacing (3.9) in (2.3) we have

$$\mathcal{J}(u) = \frac{1}{2} \int_\Omega \sigma(u) \cdot (\nabla u_\varepsilon)^s \, dx - \frac{1}{2} \int_\Omega \alpha \, p \operatorname{div}(u_\varepsilon + u) \, dx \, . \tag{3.10}$$

In the same way, taking $\eta = u_\varepsilon - u$ in (3.8), it follows that

$$\int_\Omega \sigma_\varepsilon(u_\varepsilon) \cdot (\nabla u_\varepsilon)^s \, dx = \int_\Omega \sigma_\varepsilon(u_\varepsilon) \cdot (\nabla u)^s \, dx + \int_\Omega \alpha_\varepsilon \, p \operatorname{div}(u_\varepsilon - u) \, dx \, . \tag{3.11}$$

After replacing (3.11) in (3.7) we get

$$\mathcal{J}_\varepsilon(u_\varepsilon) = \frac{1}{2} \int_\Omega \sigma_\varepsilon(u_\varepsilon) \cdot (\nabla u)^s \, dx - \frac{1}{2} \int_\Omega \alpha_\varepsilon \, p \operatorname{div}(u_\varepsilon + u) \, dx \, . \tag{3.12}$$

Now, taking into account the expressions (3.10) and (3.12), the variation of the energy shape functionals can be written as

$$\mathcal{J}_\varepsilon(u_\varepsilon) - \mathcal{J}(u) = \frac{1}{2} \int_\Omega \sigma_\varepsilon(u_\varepsilon) \cdot (\nabla u)^s \, dx - \frac{1}{2} \int_\Omega \sigma(u_\varepsilon) \cdot (\nabla u)^s \, dx$$
$$- \frac{1}{2} \int_\Omega \alpha_\varepsilon \, p \operatorname{div}(u_\varepsilon + u) \, dx + \frac{1}{2} \int_\Omega \alpha \, p \operatorname{div}(u_\varepsilon + u) \, dx \, . \tag{3.13}$$

After applying the definitions of the contrasts γ_ε and $\gamma_\varepsilon^\alpha$ given by (3.3) and (3.4), respectively, we have

$$\mathcal{J}_\varepsilon(u_\varepsilon) - \mathcal{J}(u) = \frac{1}{2} \int_{\Omega \setminus B_\varepsilon} \sigma(u_\varepsilon) \cdot (\nabla u)^s \, dx + \frac{1}{2} \int_{B_\varepsilon} \gamma \sigma(u_\varepsilon) \cdot (\nabla u)^s \, dx$$
$$- \frac{1}{2} \int_{\Omega \setminus B_\varepsilon} \sigma(u_\varepsilon) \cdot (\nabla u)^s \, dx - \frac{1}{2} \int_{B_\varepsilon} \sigma(u_\varepsilon) \cdot (\nabla u)^s \, dx$$
$$- \frac{1}{2} \int_{\Omega \setminus B_\varepsilon} \alpha \, p \operatorname{div}(u_\varepsilon + u) \, dx - \frac{1}{2} \int_{B_\varepsilon} \gamma^\alpha \alpha \, p \operatorname{div}(u_\varepsilon + u) \, dx$$
$$+ \frac{1}{2} \int_{\Omega \setminus B_\varepsilon} \alpha \, p \operatorname{div}(u_\varepsilon + u) \, dx + \frac{1}{2} \int_{B_\varepsilon} \alpha \, p \operatorname{div}(u_\varepsilon + u) \, dx \, . \tag{3.14}$$

By adding and subtracting

$$- \frac{1 - \gamma^\alpha}{2} \int_{B_\varepsilon} \alpha \, p \operatorname{div}(u) \, dx \, , \tag{3.15}$$

the following expression is obtained after canceling of the identical terms

$$\mathcal{J}_\varepsilon(u_\varepsilon) - \mathcal{J}(u) = - \frac{1 - \gamma}{2\gamma} \int_{B_\varepsilon} \sigma_\varepsilon(u_\varepsilon) \cdot (\nabla u)^s \, dx$$
$$+ \frac{1 - \gamma^\alpha}{2} \int_{B_\varepsilon} \alpha \, p \operatorname{div}(u_\varepsilon - u) \, dx + (1 - \gamma^\alpha) \int_{B_\varepsilon} \alpha \, p \operatorname{div}(u) \, dx \, . \tag{3.16}$$

Now, in order to apply the topological derivative definition, it is necessary first to know the asymptotic behavior of the function u_ε with respect to the parameter ε. To this end, let us consider the following ansatz:

$$u_\varepsilon = u + w_\varepsilon + \tilde{u}_\varepsilon \, , \tag{3.17}$$

where u is solution to the unperturbed problem (2.4), w_ε is solution to an auxiliary exterior problem and $\tilde{u}_\varepsilon$ is the remainder.

In particular, the following auxiliary boundary value problem is considered when $\varepsilon \to 0$: Find $S_\varepsilon(w_\varepsilon)$, such that

$$
\begin{cases}
\mathrm{div}\, S_\varepsilon(w_\varepsilon) & = & 0 & \text{in} & \mathbb{R}^2, \\
S_\varepsilon(w_\varepsilon) & \to & 0 & \text{in} & \infty, \\
[\![S_\varepsilon(w_\varepsilon)]\!]\, n & = & g & \text{on} & \partial B_\varepsilon,
\end{cases}
\tag{3.18}
$$

where $S_\varepsilon(w_\varepsilon) = \gamma_\varepsilon \mathbb{C}(\nabla w_\varepsilon)^s$ and $g = [\rho^{-1}(1 - \gamma^\alpha)\alpha p(\hat{x})I - (1 - \gamma)S(u)(\hat{x})]n$ obtained after adding and subtracting $\sigma(u(x))$ and $p(x)$ at the point $\hat{x}$, with $S(u) = \mathbb{C}(\nabla u)^s$. The boundary value problem (3.18) admits an explicit solution. For the case $p(x) = 0\, \forall x \in \Omega$ see [22], for instance. For the situation with constant pressure confined at the inclusion see [19]. For the present case, taking into account that the stress $S_\varepsilon(w_\varepsilon)$ is uniform inside the inclusion B_ε, the solution of (3.18) can be written in the following way

$$
S_\varepsilon(w_\varepsilon)_{|B_\varepsilon} = \mathbb{T}_\gamma S(u)(\hat{x}) + \rho^{-1}T_\gamma,
\tag{3.19}
$$

where $\mathbb{T}_\gamma$ and T_γ are fourth and second order isotropic tensors, respectively. The tensor $\mathbb{T}_\gamma$ is given by

$$
\mathbb{T}_\gamma = \frac{\gamma(1 - \gamma)}{2(1 + b\gamma)}\left(2b\mathbb{I} + \frac{a - b}{1 + a\gamma}I \otimes I \right)
\tag{3.20}
$$

and T_γ is written as

$$
T_\gamma = -(1 - \gamma^\alpha)\alpha\, p(\hat{x})\frac{a\gamma}{1 + a\gamma}I.
\tag{3.21}
$$

The constants a and b are defined in terms of the Lamé's coefficients as follows

$$
a = \frac{\lambda + \mu}{\mu} \quad \text{and} \quad b = \frac{\lambda + 3\mu}{\lambda + \mu}.
\tag{3.22}
$$

After multiplying both sides of (3.19) by the parameter ρ, we have

$$
\sigma_\varepsilon(w_\varepsilon)_{|B_\varepsilon} = \mathbb{T}_\gamma \sigma(u)(\hat{x}) + T_\gamma.
\tag{3.23}
$$

Note that the result shown in (3.23) fits the famous Eshelby's problem, see [23,24].

Let us now consider the problem associated to the term $\sigma_\varepsilon(\tilde{u}_\varepsilon)$ in order to compensate for the discrepancies introduced by the auxiliary problem (3.18). To this aim, the remainder $\tilde{u}_\varepsilon$ is solution to the following boundary value problem: Find $\tilde{u}_\varepsilon$, such that

$$
\begin{cases}
\mathrm{div}\,\sigma_\varepsilon(\tilde{u}_\varepsilon) & = & g_0 \chi_{B_\varepsilon} & \text{in} & \Omega, \\
\sigma_\varepsilon(\tilde{u}_\varepsilon) & = & \gamma_\varepsilon \rho \mathbb{C}(\nabla \tilde{u}_\varepsilon)^s, \\
\tilde{u}_\varepsilon & = & g_1 & \text{on} & \partial\Omega, \\
\left.\begin{array}{r} [\![\tilde{u}_\varepsilon]\!] = 0 \\ [\![\sigma_\varepsilon(\tilde{u}_\varepsilon)]\!]\, n = g_2 \end{array}\right\} & & & \text{on} & \partial\omega, \\
\left.\begin{array}{r} [\![\tilde{u}_\varepsilon]\!] = 0 \\ [\![\sigma_\varepsilon(\tilde{u}_\varepsilon)]\!]\, n = h \end{array}\right\} & & & \text{on} & \partial B_\varepsilon,
\end{cases}
\tag{3.24}
$$

where $g_0 = (\gamma^\alpha - \gamma)\alpha \nabla p$, $g_1 = -w_\varepsilon$, $g_2 = -(1 - \rho_0)\, S(w_\varepsilon)n$ and the term h is defined as: $h = \tilde{\sigma}n$, with $\tilde{\sigma} = (1 - \gamma^\alpha)\alpha\, (p - p(\hat{x}))I - (1 - \gamma)(\sigma(u) - \sigma(u)(\hat{x}))$. The estimate $\|\tilde{u}_\varepsilon\|_{H^1(\Omega;\mathbb{R}^2)} = O(\varepsilon^2)$ holds true.

Lemma 1. *Let $\tilde{u}_\varepsilon$ be the solution of (3.24) or, equivalently, solution to the following variational problem: Find $\tilde{u}_\varepsilon \in \tilde{\mathcal{U}}_\varepsilon$, such that*

$$
\int_\Omega \sigma_\varepsilon(\tilde{u}_\varepsilon) \cdot (\nabla \eta)^s\, dx = -\int_{B_\varepsilon} (\gamma^\alpha - \gamma)\alpha \nabla p \cdot \eta\, dx
$$

$$
-(1 - \rho_0) \int_{\partial\omega} S(w_\varepsilon)n \cdot \eta\, dx + \int_{\partial B_\varepsilon} h \cdot \eta\, dx, \quad \forall \eta \in \tilde{\mathcal{V}}_\varepsilon.
\tag{3.25}
$$

The set $\tilde{\mathcal{U}}_\varepsilon$ and the space $\tilde{\mathcal{V}}_\varepsilon$ are defined as

$$\tilde{\mathcal{U}}_\varepsilon := \left\{ \varphi \in H^1(\Omega; \mathbb{R}^2) : [\![\varphi]\!]_{|B_\varepsilon} = 0, \quad \varphi_{|\partial\Omega} = \varepsilon^2 g \right\}, \tag{3.26}$$

$$\tilde{\mathcal{V}}_\varepsilon := \left\{ \varphi \in H^1(\Omega; \mathbb{R}^2) : [\![\varphi]\!]_{|B_\varepsilon} = 0, \quad \varphi_{|\partial\Omega} = 0 \right\}, \tag{3.27}$$

with $g = -\varepsilon^{-2} w_\varepsilon$. Then, the estimate $\|\tilde{u}_\varepsilon\|_{H^1(\Omega;\mathbb{R}^2)} = O(\varepsilon^2)$ holds true.

Proof. From the definition of function $h = \tilde{\sigma} n$, with n used to denote the unit normal vector field on ∂B_ε pointing toward the center of the inclusion, we have

$$\int_{\partial B_\varepsilon} h \cdot \eta \, dx = \int_{B_\varepsilon} (\gamma^\alpha - \gamma)\alpha \nabla p \cdot \eta \, dx - \int_{B_\varepsilon} (1 - \gamma^\alpha)\alpha (p - p(\hat{x}))\mathrm{div}(\eta) \, dx$$
$$+ \int_{B_\varepsilon} (1 - \gamma)(\sigma(u) - \sigma(u)(\hat{x})) \cdot (\nabla\eta)^s \, dx, \tag{3.28}$$

where we have taken into account that $\tilde{\sigma} = (1-\gamma^\alpha)\alpha(p-p(\hat{x}))\mathrm{I} - (1-\gamma)(\sigma(u)-\sigma(u)(\hat{x}))$ and that $\mathrm{div}(\sigma(u)) = \alpha\nabla p$, which comes out from the variational form (2.4). From this last result, the variational form (3.25) can be rewritten as follows

$$\int_\Omega \sigma_\varepsilon(\tilde{u}_\varepsilon) \cdot (\nabla\eta)^s \, dx = \int_{B_\varepsilon} (1-\gamma)(\sigma(u) - \sigma(u)(\hat{x})) \cdot (\nabla\eta)^s \, dx - (1-\rho_0)\int_{\partial\omega} S(w_\varepsilon)n \cdot \eta \, dx$$
$$- \int_{B_\varepsilon} (1-\gamma^\alpha)\alpha(p - p(\hat{x}))\mathrm{div}(\eta) \, dx, \quad \forall \eta \in \tilde{\mathcal{V}}_\varepsilon. \tag{3.29}$$

By taking $\eta = \tilde{u}_\varepsilon - \varphi_\varepsilon$ in (3.29), with $\varphi_\varepsilon \in \tilde{\mathcal{U}}_\varepsilon$, from the strong form (3.24), we have

$$\int_\Omega \sigma_\varepsilon(\tilde{u}_\varepsilon) \cdot (\nabla\tilde{u}_\varepsilon)^s \, dx = \varepsilon^2 \int_{\partial\Omega} \sigma_\varepsilon(\tilde{u}_\varepsilon)n \cdot g \, dx + \int_{B_\varepsilon} (1-\gamma)(\sigma(u) - \sigma(u)(\hat{x})) \cdot (\nabla\tilde{u}_\varepsilon)^s \, dx$$
$$- \int_{B_\varepsilon} (1-\gamma^\alpha)\alpha(p - p(\hat{x}))\mathrm{div}(\tilde{u}_\varepsilon) \, dx - (1-\rho_0)\int_{\partial\omega} S(w_\varepsilon)n \cdot \tilde{u}_\varepsilon \, dx. \tag{3.30}$$

Then, by applying the Cauchy–Schwarz inequality, it follows that

$$\int_\Omega \sigma_\varepsilon(\tilde{u}_\varepsilon) \cdot (\nabla\tilde{u}_\varepsilon)^s \, dx \leq \varepsilon^2 \|\sigma_\varepsilon(\tilde{u}_\varepsilon)n\|_{H^{-1/2}(\partial\Omega;\mathbb{R}^2)} \|g\|_{H^{1/2}(\partial\Omega;\mathbb{R}^2)}$$
$$+ c_1 \|\sigma(u) - \sigma(u)(\hat{x})\|_{L^2(B_\varepsilon;\mathbb{R}^2)} \|\nabla\tilde{u}_\varepsilon\|_{L^2(B_\varepsilon;\mathbb{R}^2)}$$
$$+ c_2 \|p - p(\hat{x})\|_{L^2(B_\varepsilon)} \|\nabla\tilde{u}_\varepsilon\|_{L^2(B_\varepsilon;\mathbb{R}^2)}$$
$$+ c_3 \|S(w_\varepsilon)n\|_{H^{-1/2}(\partial\omega;\mathbb{R}^2)} \|\tilde{u}_\varepsilon\|_{H^{1/2}(\partial\omega;\mathbb{R}^2)}. \tag{3.31}$$

By applying the trace theorem it follows that

$$\int_\Omega \sigma_\varepsilon(\tilde{u}_\varepsilon) \cdot (\nabla\tilde{u}_\varepsilon)^s \, dx \leq c_4(\varepsilon^2 + \|x - \hat{x}\|_{L^2(B_\varepsilon;\mathbb{R}^2)}) \|\tilde{u}_\varepsilon\|_{H^1(\Omega;\mathbb{R}^2)}$$
$$\leq c_5\varepsilon^2 \|\tilde{u}_\varepsilon\|_{H^1(\Omega;\mathbb{R}^2)}, \tag{3.32}$$

where we have used the interior elliptic regularity of functions u and p together with the fact that the explicit solution $S(w_\varepsilon)$ is of order $O(\varepsilon^2)$ far from the inclusion B_ε [22]. Finally, from the coercivity of the bilinear form on the left hand side of the above inequality, we have

$$c \|\tilde{u}_\varepsilon\|^2_{H^1(\Omega;\mathbb{R}^2)} \leq \int_\Omega \sigma_\varepsilon(\tilde{u}_\varepsilon) \cdot (\nabla\tilde{u}_\varepsilon)^s \, dx. \tag{3.33}$$

Then, it follows immediately that

$$\|\tilde{u}_\varepsilon\|_{H^1(\Omega;\mathbb{R}^2)} \leq C\varepsilon^2, \tag{3.34}$$

where $C = c_5/c$ is a constant independent of the small parameter ε. $\quad\square$

Now, the integrals in (3.16) can be evaluated explicitly. In fact, after replacing the ansatz for u_ε given by (3.17) in the first integral of the (3.16) we have

$$\int_{B_\varepsilon} \sigma_\varepsilon(u_\varepsilon) \cdot (\nabla u)^s \, dx = \underbrace{\int_{B_\varepsilon} \sigma_\varepsilon(u) \cdot (\nabla u)^s \, dx}_{(a)} + \underbrace{\int_{B_\varepsilon} \sigma_\varepsilon(w_\varepsilon) \cdot (\nabla u)^s \, dx}_{(b)} + \mathcal{E}_1(\varepsilon) . \tag{3.35}$$

The remainder $\mathcal{E}_1(\varepsilon)$ is given by

$$\mathcal{E}_1(\varepsilon) = \int_{B_\varepsilon} \sigma_\varepsilon(\tilde{u}_\varepsilon) \cdot (\nabla u)^s \, dx ,$$
$$|\mathcal{E}_1(\varepsilon)| \leq \|\sigma_\varepsilon(\tilde{u}_\varepsilon)\|_{L^2(B_\varepsilon;\mathbb{R}^2)} \|\nabla u\|_{L^2(B_\varepsilon;\mathbb{R}^2)}$$
$$\leq c_1 \varepsilon \|\tilde{u}_\varepsilon\|_{H^1(\Omega;\mathbb{R}^2)} \leq c_2 \varepsilon^3 = o(\varepsilon^2) , \tag{3.36}$$

where we have used the Cauchy–Schwarz inequality together with the obtained estimate to the remainder $\tilde{u}_\varepsilon$. The term (a) in (3.35) can be developed in terms of ε as follows

$$\int_{B_\varepsilon} \sigma_\varepsilon(u) \cdot (\nabla u)^s \, dx = \int_{B_\varepsilon} \gamma \sigma(u) \cdot (\nabla u)^s \, dx$$
$$= \pi \varepsilon^2 \gamma \sigma(u)(\hat{x}) \cdot (\nabla u)^s(\hat{x}) + \mathcal{E}_2(\varepsilon) . \tag{3.37}$$

The remainder $\mathcal{E}_2(\varepsilon)$ is given by

$$\mathcal{E}_2(\varepsilon) = \int_{B_\varepsilon} (h - h(\hat{x})) \, dx ,$$
$$|\mathcal{E}_2(\varepsilon)| \leq c_1 \varepsilon \|x - \hat{x}\|_{L^2(B_\varepsilon;\mathbb{R}^2)} \leq c_2 \varepsilon^3 = o(\varepsilon^2) , \tag{3.38}$$

where the notation

$$h - h(\hat{x}) = \gamma (\sigma(u) \cdot (\nabla u)^s - \sigma(u)(\hat{x}) \cdot (\nabla u)^s(\hat{x})) , \tag{3.39}$$

has been introduced. Note that we have used again the Cauchy–Schwarz inequality and, then, the interior elliptic regularity of the solution u. Since the exact solution to the exterior problem (3.18) is known, the term (b) in (3.35) can be written as

$$\int_{B_\varepsilon} \sigma_\varepsilon(w_\varepsilon) \cdot (\nabla u)^s \, dx = \pi \varepsilon^2 (\nabla u)^s(\hat{x}) \cdot (\mathbb{T}_\gamma \sigma(u)(\hat{x}) + \mathrm{T}_\gamma) + \mathcal{E}_3(\varepsilon) . \tag{3.40}$$

The remainder $\mathcal{E}_3(\varepsilon)$ is given by

$$\mathcal{E}_3(\varepsilon) = \int_{B_\varepsilon} \sigma_\varepsilon(w_\varepsilon) \cdot ((\nabla u)^s - (\nabla u)^s(\hat{x})) \, dx ,$$
$$|\mathcal{E}_3(\varepsilon)| \leq \|\sigma_\varepsilon(w_\varepsilon)\|_{L^2(B_\varepsilon;\mathbb{R}^2)} \|\nabla u - \nabla u(\hat{x})\|_{L^2(B_\varepsilon;\mathbb{R}^2)}$$
$$\leq c_1 \varepsilon \|x - \hat{x}\|_{L^2(B_\varepsilon;\mathbb{R}^2)} \leq c_2 \varepsilon^3 = o(\varepsilon^2) , \tag{3.41}$$

where we have used again the Cauchy–Schwarz inequality and the interior elliptic regularity of the solution u.

By replacing the ansatz for u_ε given by (3.17) in the second integral of (3.16) we obtain

$$\int_{B_\varepsilon} \alpha \, p \, \mathrm{div}(u_\varepsilon - u) \, dx = \int_{B_\varepsilon} \alpha \, p \, \mathrm{div}(w_\varepsilon + \tilde{u}_\varepsilon) \, dx$$
$$= \int_{B_\varepsilon} \alpha \, p(\hat{x}) \, \mathrm{div}(w_\varepsilon) \, dx + \mathcal{E}_4(\varepsilon) + \mathcal{E}_5(\varepsilon) . \tag{3.42}$$

The remainder $\mathcal{E}_4(\varepsilon)$ is given by

$$\mathcal{E}_4(\varepsilon) = \int_{B_\varepsilon} \alpha \, (p - p(\hat{x})) \, \mathrm{div}(w_\varepsilon) \, dx ,$$
$$|\mathcal{E}_4(\varepsilon)| \leq c_1 \|x - \hat{x}\|_{L^2(B_\varepsilon;\mathbb{R}^2)} \|\sigma_\varepsilon(w_\varepsilon)\|_{L^2(B_\varepsilon;\mathbb{R}^2)} \leq c_2 \varepsilon^3 = o(\varepsilon^2) , \tag{3.43}$$

where we have used the interior elliptic regularity of the function p and the solution to the problem (3.18). For the remainder $\mathcal{E}_5(\varepsilon)$ we have the following estimate

$$\mathcal{E}_5(\varepsilon) = \int_{B_\varepsilon} \alpha\, p\, \mathrm{div}(\tilde{u}_\varepsilon)\, dx\ ,$$

$$|\mathcal{E}_5(\varepsilon)| \leq c_1 \|p\|_{L^2(B_\varepsilon)} \|\nabla \tilde{u}_\varepsilon\|_{L^2(B_\varepsilon;\mathbb{R}^2)}$$

$$\leq c_2 \varepsilon \|\tilde{u}_\varepsilon\|_{H^1(\Omega;\mathbb{R}^2)} \leq c_2 \varepsilon^3 = o(\varepsilon^2)\ . \tag{3.44}$$

By using the constitutive relation and some algebraic manipulation, we obtain

$$\int_{B_\varepsilon} \alpha\, p(\hat{x})\, \mathrm{div}(w_\varepsilon)\, dx = \int_{B_\varepsilon} \alpha\, p(\hat{x}) \frac{1}{2\rho\gamma(\mu+\lambda)} \mathrm{tr}\sigma_\varepsilon(w_\varepsilon)\, dx\ , \tag{3.45}$$

where $\mathrm{tr}\sigma_\varepsilon(w_\varepsilon)$, evaluated inside the inclusion, is written as

$$\mathrm{tr}\sigma_\varepsilon(w_\varepsilon)|_{B_\varepsilon(\hat{x})} = \frac{a\gamma}{1+a\gamma}[(1-\gamma)\mathrm{tr}\sigma(u)(\hat{x}) - 2(1-\gamma^\alpha)\alpha\, p(\hat{x})]\ . \tag{3.46}$$

The last term in (3.16) can be developed as follows

$$\int_{B_\varepsilon} \alpha\, p\, \mathrm{div}(u)\, dx = \pi\varepsilon^2 \alpha\, p(\hat{x})\, \mathrm{div}(u)(\hat{x}) + \mathcal{E}_6(\varepsilon)\ , \tag{3.47}$$

with the remainder $\mathcal{E}_6(\varepsilon)$ defined as

$$\mathcal{E}_6(\varepsilon) = \int_{B_\varepsilon} (h - h(\hat{x}))\, dx\ ,$$

$$|\mathcal{E}_6(\varepsilon)| \leq c_1 \varepsilon \|x - \hat{x}\|_{L^2(B_\varepsilon;\mathbb{R}^2)} \leq c_2 \varepsilon^3 = o(\varepsilon^2)\ , \tag{3.48}$$

where the following notation has been introduced

$$h - h(\hat{x}) = \alpha\, p\, \mathrm{div}(u)(x) - \alpha\, p(\hat{x})\, \mathrm{div}(u)(\hat{x})\ . \tag{3.49}$$

Note that we have used the Cauchy–Schwarz inequality and the interior elliptic regularity of the solutions u and p.

From the above results, the variation of the energy shape functionals, given by (3.16), can be rewritten as

$$\mathcal{J}_\varepsilon(u_\varepsilon) - \mathcal{J}(u) = -\pi\varepsilon^2 \frac{1-\gamma}{2\gamma} \left[\gamma\sigma(u)(\hat{x}) + (\mathbb{T}_\gamma\sigma(u)(\hat{x}) + \mathrm{T}_\gamma) \right] \cdot (\nabla u)^s(\hat{x})$$

$$+ \pi\varepsilon^2 \frac{a}{2} \frac{1-\gamma}{1+a\gamma} (1-\gamma^\alpha)\alpha\, p(\hat{x})\, \mathrm{div}(u)(\hat{x}) + \pi\varepsilon^2(1-\gamma^\alpha)\alpha\, p(\hat{x})\, \mathrm{div}(u)(\hat{x})$$

$$- \pi\varepsilon^2 \frac{(1-\gamma^\alpha)^2}{2\rho\mu(1+a\gamma)}\alpha^2\, p(\hat{x})^2 + \sum_{i=1}^{6} \mathcal{E}_i(\varepsilon)\ , \tag{3.50}$$

where $|\mathcal{E}_i(\varepsilon)| = o(\varepsilon^2)$, for $i = 1, \ldots, 6$, as shown. Rearranging the above terms, the following expression is obtained

$$\mathcal{J}_\varepsilon(u_\varepsilon) - \mathcal{J}(u) = \pi\varepsilon^2 \mathbb{P}_\gamma\sigma(u)(\hat{x}) \cdot (\nabla u)^s(\hat{x})$$

$$+\pi\varepsilon^2 \frac{1+a}{1+a\gamma}(1-\gamma^\alpha)\alpha\, p(\hat{x})\, \mathrm{div}(u)(\hat{x}) - \pi\varepsilon^2 \frac{(1-\gamma^\alpha)^2}{2\rho\mu(1+a\gamma)}\alpha^2\, p(\hat{x})^2 + \sum_{i=1}^{6} \mathcal{E}_i(\varepsilon)\ , \tag{3.51}$$

where $\mathbb{P}_\gamma$ is given

$$\mathbb{P}_\gamma = -\frac{1}{2} \frac{1-\gamma}{1+b\gamma} \left((1+b)\mathbb{I} + \frac{1}{2}(a-b)\frac{1-\gamma}{1+a\gamma} \mathrm{I} \otimes \mathrm{I} \right)\ , \tag{3.52}$$

with the coefficients a and b defined by (3.22).

3.2. Perturbation on the permeability

Now, we consider $\gamma^f \neq 1$ with $\gamma = \gamma^\alpha = 1$. In this case, the total energy of the perturbed system $\mathcal{J}_\varepsilon(u_\varepsilon)$ is given by

$$\mathcal{J}_\varepsilon(u_\varepsilon) = \frac{1}{2} \int_\Omega \sigma(u_\varepsilon) \cdot (\nabla u_\varepsilon)^s\, dx - \int_\Omega \alpha p_\varepsilon\, \mathrm{div}(u_\varepsilon)\, dx\ , \tag{3.53}$$

with the vector function u_ε solution to the following variational problem: Find $u_\varepsilon \in \mathcal{U}$, such that

$$\int_\Omega \sigma(u_\varepsilon) \cdot (\nabla \eta)^s \, dx = \int_\Omega \alpha p_\varepsilon \operatorname{div}(\eta) \, dx \, , \ \forall \eta \in \mathcal{V}, \tag{3.54}$$

where p_ε is solution to the problem: Find $p_\varepsilon \in \mathcal{P}$, such that

$$\int_\Omega k_\varepsilon \nabla p_\varepsilon \cdot \nabla \varphi \, dx = 0 \, , \ \forall \varphi \in \mathcal{Q} \, , \tag{3.55}$$

with $k_\varepsilon = \gamma_\varepsilon^f k$, where γ_ε^f is given by (3.5).

Again, in order to evaluate the difference between the energy shape functionals $\mathcal{J}(u)$ and $\mathcal{J}_\varepsilon(u_\varepsilon)$, which are now defined through (2.3) and (3.53), respectively, we take first $\eta = u_\varepsilon - u$ as test function in problem (2.4). Then, the following equality is obtained

$$\int_\Omega \sigma(u) \cdot (\nabla u)^s \, dx = \int_\Omega \sigma(u) \cdot (\nabla u_\varepsilon)^s \, dx - \int_\Omega \alpha \, p \operatorname{div}(u_\varepsilon - u) \, dx \, . \tag{3.56}$$

By replacing (3.56) in (2.3) we have

$$\mathcal{J}(u) = \frac{1}{2} \int_\Omega \sigma(u) \cdot (\nabla u_\varepsilon)^s \, dx - \frac{1}{2} \int_\Omega \alpha \, p \operatorname{div}(u_\varepsilon + u) \, dx \, . \tag{3.57}$$

In the same way, let us take $\eta = u_\varepsilon - u$ as test function in (3.54) to obtain

$$\int_\Omega \sigma(u_\varepsilon) \cdot (\nabla u_\varepsilon)^s \, dx = \int_\Omega \sigma(u_\varepsilon) \cdot (\nabla u)^s \, dx + \int_\Omega \alpha \, p_\varepsilon \operatorname{div}(u_\varepsilon - u) \, dx \, . \tag{3.58}$$

After replacing (3.58) in (3.53) we get

$$\mathcal{J}_\varepsilon(u_\varepsilon) = \frac{1}{2} \int_\Omega \sigma(u_\varepsilon) \cdot (\nabla u)^s \, dx - \frac{1}{2} \int_\Omega \alpha \, p_\varepsilon \operatorname{div}(u_\varepsilon + u) \, dx \, . \tag{3.59}$$

From Eqs. (3.57) and (3.59), the variation of the energy shape functionals is written as

$$\mathcal{J}_\varepsilon(u_\varepsilon) - \mathcal{J}(u) = -\frac{1}{2} \int_\Omega \alpha \, (p_\varepsilon - p) \operatorname{div}(u_\varepsilon + u) \, dx \, . \tag{3.60}$$

At this point, we write $u_\varepsilon + u = 2u + (u_\varepsilon - u)$ to obtain

$$\mathcal{J}_\varepsilon(u_\varepsilon) - \mathcal{J}(u) = -\int_\Omega \alpha \, (p_\varepsilon - p) \operatorname{div}(u) \, dx + \mathcal{E}_7(\varepsilon) \, , \tag{3.61}$$

where

$$\mathcal{E}_7(\varepsilon) = -\frac{1}{2} \int_\Omega \alpha \, (p_\varepsilon - p) \operatorname{div}(u_\varepsilon - u) \, dx \, . \tag{3.62}$$

The estimate $|\mathcal{E}_7(\varepsilon)| = o(\varepsilon^2)$ holds true and will be verified in the next two Lemmas.

By subtracting (2.5) of (3.55) and applying the definition of the contrast γ_ε^f given by (3.5), the following expression is obtained

$$\int_{\Omega \setminus B_\varepsilon} k \nabla p_\varepsilon \cdot \nabla \varphi \, dx + \int_{B_\varepsilon} \gamma^f k \nabla p_\varepsilon \cdot \nabla \varphi \, dx - \int_{\Omega \setminus B_\varepsilon} k \nabla p \cdot \nabla \varphi \, dx - \int_{B_\varepsilon} k \nabla p \cdot \nabla \varphi \, dx = 0 \, . \tag{3.63}$$

By adding and subtracting the term

$$\int_{B_\varepsilon} k \nabla (p_\varepsilon - p) \cdot \nabla \varphi \, dx \, , \tag{3.64}$$

after canceling the identical terms, we obtain the following equality

$$\int_\Omega k \nabla (p_\varepsilon - p) \cdot \nabla \varphi \, dx = (1 - \gamma^f) \int_{B_\varepsilon} k \nabla p_\varepsilon \cdot \nabla \varphi \, dx \, . \tag{3.65}$$

Finally, by taking $\varphi = p_\varepsilon - p$ in (2.15) and $\varphi = q$ in (3.65), with q solution of (2.15), expansion (3.61) can be conveniently rewritten as

$$\mathcal{J}_\varepsilon(u_\varepsilon) - \mathcal{J}(u) = -(1 - \gamma^f) \int_{B_\varepsilon} k \nabla p_\varepsilon \cdot \nabla q \, dx \, . \tag{3.66}$$

Now, it is necessary to know the asymptotic behavior of the solution p_ε with respect to the small parameter ε. To this end, let us propose the following ansatz:

$$p_\varepsilon = p + w_\varepsilon^p + \tilde{p}_\varepsilon \,, \tag{3.67}$$

where p is solution to the unperturbed problem (2.5), w_ε^p is solution to an auxiliary exterior problem and $\tilde{p}_\varepsilon$ is the remainder.

The auxiliary exterior problem is defined as: Find $w_\varepsilon^p(x)$, such that

$$\begin{cases} \operatorname{div}(\gamma_\varepsilon^f \nabla w_\varepsilon^p) & = & 0 & \text{in} & \mathbb{R}^2 \,, \\ w_\varepsilon^p & \to & 0 & \text{in} & \infty \,, \\ \left.\begin{array}{rcl} [\![w_\varepsilon^p]\!] & = & 0 \\ [\![\gamma_\varepsilon^f \nabla w_\varepsilon^p]\!] \cdot n & = & g \end{array}\right\} & & & \text{on} & \partial B_\varepsilon \,, \end{cases} \tag{3.68}$$

with $g = -(1 - \gamma^f)\nabla p(\hat{x}) \cdot n$ obtained from Taylor series expansion of $p(x)$ around the point $\hat{x}$. The problem (3.68) has an explicit solution, namely

$$w_\varepsilon^p(x)_{|\mathbb{R}^2 \setminus \overline{B_\varepsilon}} = \frac{1 - \gamma^f}{1 + \gamma^f} \frac{\varepsilon^2}{\|x - \hat{x}\|^2} \nabla p(\hat{x}) \cdot (x - \hat{x}) \,, \tag{3.69}$$

$$w_\varepsilon^p(x)_{|B_\varepsilon} = \frac{1 - \gamma^f}{1 + \gamma^f} \nabla p(\hat{x}) \cdot (x - \hat{x}) \,. \tag{3.70}$$

For more details about the problem (3.68) and its solution see [22, Ch. 5, pp. 144], where the estimate $\|\tilde{p}_\varepsilon\|_{H^1(\Omega)} = O(\varepsilon^2)$ can also be verified.

The next two results ensure the existence of the topological derivative associated with the case analyzed in this section.

Lemma 2. *Let p and p_ε be the solutions of (2.5) and (3.55), respectively. Then, the following estimate holds true:*

$$\|p_\varepsilon - p\|_{L^2(\Omega)} = o(\varepsilon). \tag{3.71}$$

Proof. From the ansatz (3.67) proposed to p_ε, and by applying the triangular inequality together with the known estimate for $\tilde{p}_\varepsilon$, we obtain

$$\|p_\varepsilon - p\|_{L^2(\Omega)} \leq \|w_\varepsilon^p\|_{L^2(\Omega)} + O(\varepsilon^2) \,. \tag{3.72}$$

By defining a ball $B_R(\hat{x})$ of radius R and center in $\hat{x} \in \Omega$, so that $B_R(\hat{x}) \supset \Omega$, the following result is obtained

$$\begin{aligned} \|w_\varepsilon^p\|_{L^2(\Omega)} &\leq \|w_\varepsilon^p\|_{L^2(B_R)} \\ &= \left(\int_{B_R \setminus B_\varepsilon} |w_\varepsilon^p|^2 \, dx + \int_{B_\varepsilon} |w_\varepsilon^p|^2 \, dx \right)^{1/2} \,. \end{aligned} \tag{3.73}$$

From w_ε^p given by (3.69) and (3.70), we can evaluate explicitly the integrals in (3.73), namely

$$\|w_\varepsilon^p\|_{L^2(B_R)} \leq c\varepsilon^2 \sqrt{|\log(\varepsilon)|} = o(\varepsilon) \,. \tag{3.74}$$

Then,

$$\|p_\varepsilon - p\|_{L^2(\Omega)} = o(\varepsilon) + O(\varepsilon^2) = o(\varepsilon) \,. \quad \square \tag{3.75}$$

Lemma 3. *Let u and u_ε be the solutions of (2.4) and (3.54), respectively. Then, the following estimate holds true:*

$$\|u_\varepsilon - u\|_{H^1(\Omega;\mathbb{R}^2)} = o(\varepsilon). \tag{3.76}$$

Proof. By subtracting (2.4) from (3.54) and taking $\eta = u_\varepsilon - u$ it follows that

$$\int_\Omega \sigma(u_\varepsilon - u) \cdot \nabla(u_\varepsilon - u)^s \, dx = \int_\Omega \alpha(p_\varepsilon - p) \operatorname{div}(u_\varepsilon - u) \, dx \, . \tag{3.77}$$

The application of the Cauchy–Schwarz inequality leads to

$$\int_\Omega \sigma(u_\varepsilon - u) \cdot \nabla(u_\varepsilon - u)^s \, dx \le C_1 \|p_\varepsilon - p\|_{L^2(\Omega)} \|\nabla(u_\varepsilon - u)\|_{L^2(\Omega;\mathbb{R}^2)}$$

$$\le C_1 \|p_\varepsilon - p\|_{L^2(\Omega)} \|u_\varepsilon - u\|_{H^1(\Omega;\mathbb{R}^2)} \, . \tag{3.78}$$

From the coercivity of the bilinear form at the left hand side of (3.77) we have

$$c\|u_\varepsilon - u\|^2_{H^1(\Omega;\mathbb{R}^2)} \le \int_\Omega \sigma_\varepsilon(u_\varepsilon - u) \cdot \nabla(u_\varepsilon - u)^s \, dx \, . \tag{3.79}$$

Then, taking into account Lemma 2, the proof is concluded with $C = C_1/c$ independent of the parameter ε. □

Let us come back to the definition of $\mathcal{E}_7(\varepsilon)$ given by (3.62). From the Cauchy–Schwarz inequality, we obtain

$$|\mathcal{E}_7(\varepsilon)| \le c_1 \|p_\varepsilon - p\|_{L^2(\Omega)} \|\nabla(u_\varepsilon - u)\|_{L^2(\Omega;\mathbb{R}^2)} = o(\varepsilon^2) \, , \tag{3.80}$$

where we have used Lemmas 2 and 3.

Now, replacing the ansatz (3.67) proposed to p_ε in the integral (3.66) we have

$$\int_{B_\varepsilon} k\nabla p_\varepsilon \cdot \nabla q \, dx = \underbrace{\int_{B_\varepsilon} k\nabla p \cdot \nabla q \, dx}_{(a)} + \underbrace{\int_{B_\varepsilon} k\nabla w_\varepsilon^p \cdot \nabla q \, dx}_{(b)} + \mathcal{E}_8(\varepsilon) \, . \tag{3.81}$$

The remainder $\mathcal{E}_8(\varepsilon)$ is given by

$$\mathcal{E}_8(\varepsilon) = \int_{B_\varepsilon} k\nabla \tilde{p}_\varepsilon \cdot \nabla q \, dx \, ,$$

$$|\mathcal{E}_8(\varepsilon)| \le \|k\nabla \tilde{p}_\varepsilon\|_{L^2(B_\varepsilon)} \|\nabla q\|_{L^2(B_\varepsilon)}$$

$$\le c_1 \varepsilon \|\tilde{p}_\varepsilon\|_{H^1(\Omega)} \le c_2 \varepsilon^3 = o(\varepsilon^2) \, , \tag{3.82}$$

where we have used the Cauchy–Schwarz inequality together with the known estimate to $\tilde{p}_\varepsilon$.

The term (a) in (3.81) can be developed in terms of ε as

$$\int_{B_\varepsilon} k\nabla p \cdot \nabla q \, dx = \pi \varepsilon^2 k\nabla p(\hat{x}) \cdot \nabla q(\hat{x}) + \mathcal{E}_9(\varepsilon) \, , \tag{3.83}$$

with the remainder $\mathcal{E}_9(\varepsilon)$ defined by

$$\mathcal{E}_9(\varepsilon) = \int_{B_\varepsilon} (h - h(\hat{x})) \, dx \, ,$$

$$|\mathcal{E}_9(\varepsilon)| \le c_1 \varepsilon \|x - \hat{x}\|_{L^2(B_\varepsilon;\mathbb{R}^2)} \le c_2 \varepsilon^3 = o(\varepsilon^2) \, , \tag{3.84}$$

where the notation

$$h - h(\hat{x}) = k\nabla p \cdot \nabla q - k\nabla p(\hat{x}) \cdot \nabla q(\hat{x}) \, , \tag{3.85}$$

has been introduced. In this case, we have used the Cauchy–Schwarz inequality and the interior elliptic regularity of the function p.

Since the exact solution of the auxiliary problem (3.68) is known, the term (b) in (3.81) can be written as

$$\int_{B_\varepsilon} k\nabla w_\varepsilon^p \cdot \nabla q \, dx = \pi \varepsilon^2 k\nabla w_\varepsilon^p \cdot \nabla q(\hat{x}) + \mathcal{E}_{10}(\varepsilon) \, . \tag{3.86}$$

The remainder $\mathcal{E}_{10}(\varepsilon)$ is given by

$$\mathcal{E}_{10}(\varepsilon) = \int_{B_\varepsilon} k\nabla w_\varepsilon^p \cdot (\nabla q - \nabla q(\hat{x})) \, dx \, ,$$

$$|\mathcal{E}_{10}(\varepsilon)| \le \|k\nabla w_\varepsilon^p\|_{L^2(B_\varepsilon)} \|\nabla q - \nabla q(\hat{x})\|_{L^2(B_\varepsilon)}$$

$$\le c_1 \varepsilon \|x - \hat{x}\|_{L^2(B_\varepsilon;\mathbb{R}^2)} \le c_2 \varepsilon^3 = o(\varepsilon^2) \, . \tag{3.87}$$

Therefore, from the above results, the variation (3.66) can be rewritten as

$$
\mathcal{J}_\varepsilon(u_\varepsilon) - \mathcal{J}(u) = -\pi \varepsilon^2 (1 - \gamma^f) \left[k \nabla p(\hat{x}) + k \nabla w_\varepsilon^p \right] \cdot \nabla q(\hat{x}) + \sum_{i=7}^{10} \mathcal{E}_i(\varepsilon)
$$

$$
= -\pi \varepsilon^2 \, 2 \frac{1 - \gamma^f}{1 + \gamma^f} k \nabla p(\hat{x}) \cdot \nabla q(\hat{x}) + \sum_{i=7}^{10} \mathcal{E}_i(\varepsilon) , \tag{3.88}
$$

where the remainders $|\mathcal{E}_i(\varepsilon)| = o(\varepsilon^2)$, for $i = 7, \dots, 10$, as shown.

3.3. Topological derivative formula

The topological derivative of the shape functional (2.2), with respect to the nucleation of a small circular inclusion characterized by the contrasts γ, γ^α and γ^f, is given by the following sum

$$
D_T \mathcal{F}_\omega(x) = D_T \mathcal{J}(x) + \kappa_\delta D_T |\omega|(x) \quad \forall x \in \Omega . \tag{3.89}
$$

The last term $\kappa_\delta D_T |\omega|(x)$ is trivially obtained and given by

$$
\kappa_\delta D_T |\omega|(x) = \begin{cases} +\kappa_\delta, & \text{if } x \in \Omega \setminus \overline{\omega} , \\ -\kappa_\delta, & \text{if } x \in \omega . \end{cases} \tag{3.90}
$$

The variations between the energy functionals $\mathcal{J}(u)$ and $\mathcal{J}_\varepsilon(u_\varepsilon)$ have been developed in Sections 3.1 and 3.2. From these variations, we can identify function $f(\varepsilon) = \pi \varepsilon^2$ and thus evaluate the term $D_T \mathcal{J}(x)$. In particular, by taking into account the variations (3.51) and (3.88), the topological derivative [15,16,22] of the energy shape functional is given by

$$
D_T \mathcal{J}(x) = \mathbb{P}_\gamma \sigma(u)(x) \cdot (\nabla u)^s(x) + \frac{1 + a}{1 + a\gamma}(1 - \gamma^\alpha) \alpha \, p(x) \operatorname{div}(u)(x)
$$

$$
- \frac{(1 - \gamma^\alpha)^2}{2\rho\mu(1 + a\gamma)} \alpha^2 p(x)^2 - 2 \frac{1 - \gamma^f}{1 + \gamma^f} k \nabla p(x) \cdot \nabla q(x) , \tag{3.91}
$$

with the polarization tensor $\mathbb{P}_\gamma$ given by (3.52).

In order to check for the correctness of result (3.91), we consider a domain $\Omega = (0, 1) \times (0, 1)$ m^2 representing a clamped block with a centered inclusion denoted by $B_\varepsilon(x_0)$. The Young modulus, Poisson ratio, Biot coefficient and permeability are given by $E = 17.000$ MPa, $\nu = 0, 2$, $\alpha = 0, 1$ and $k = 1, 0$ mD in $\Omega \setminus \overline{B_\varepsilon(x_0)}$ and $E = 17.000 \times 10^{-6}$ MPa, $\nu = 0, 2$, $\alpha = 1, 0$ and $k = 10^3$ mD in $B_\varepsilon(x_0)$, respectively. The adopted values for the material properties are precisely the same as in Section 5, showing the numerical experiments. The bottom of Ω is subject to a pressure of 1 MPa, whereas on its top a null pressure is prescribed. Now, let us introduce the following quantities

$$
\delta\psi(\varepsilon) := \frac{\mathcal{J}_\varepsilon(u_\varepsilon) - \mathcal{J}(u)}{|B_\varepsilon(x_0)|} \tag{3.92}
$$

$$
D_T \psi(x_0) := \lim_{\varepsilon \to 0} \delta\psi(\varepsilon). \tag{3.93}
$$

Finally, we consider $\varepsilon = 2^{-n}$, with $n = 3, \dots, 8$ integer. The problem is discretized into 105.138 linear triangular finite elements, with the mesh intensified toward the center of the inclusion. From these elements, the graph $\delta\psi(\varepsilon) \times 1/\varepsilon$ is plotted in Fig. 3. We observe that the horizontal asymptote (solid line) corresponds to the topological derivative evaluated at the center x_0 of Ω, whose value is given by $D_T \psi(x_0)$.

4. Topology optimization algorithm

The original algorithm, proposed to study the crack nucleation/propagation based only on the topological derivative field, was proposed in [18] and extended to the hydraulic fracture context in [19]. It is based on the introduction of an inclusion at the region where the topological derivative is negative. This strategy is justified by the fact that the introduction of an infinitesimal inclusion where the topological derivative is negative decreases the values of the associated shape functional. In this way, the crack path is characterized by the sequence of inclusions nucleated during the minimization process. Since several improvements with respect to the methodology presented in [19] were made, the main aspects of the new algorithm are presented in the next section.
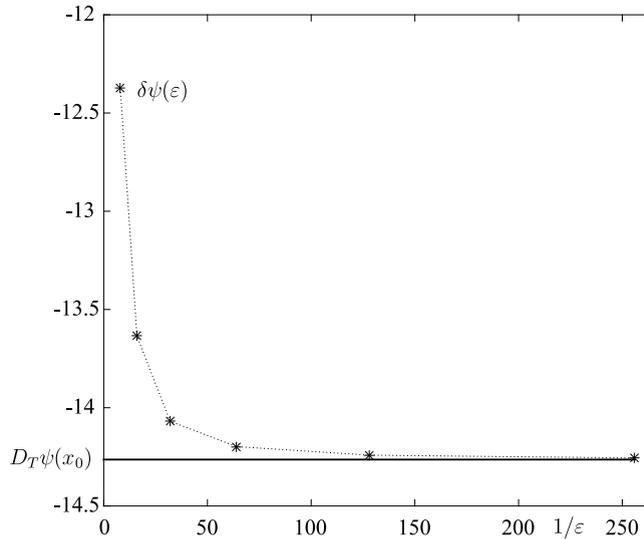
Fig. 3. Variation of the energy shape functional $\delta\psi(\varepsilon)$ from (3.92) with respect to $1/\varepsilon$.

4.1. Description of the algorithm

As mentioned, the size of the inclusion to be nucleated is associated with the region ω^* where the topological derivative is negative, i.e.,

$$\omega^* := \{x \in \Omega : D_T\mathcal{F}_\omega(x) < 0\} . \tag{4.1}$$

Let $D_T\mathcal{F}_\omega^*$ be the minimum value of the topological derivative, i.e.,

$$D_T\mathcal{F}_\omega^* := \min_{x \in \omega^*} D_T\mathcal{F}_\omega(x) . \tag{4.2}$$

The inclusion to be nucleated inside the region ω^*, denoted by ω^β, is defined as

$$\omega^\beta := \left\{x \in \omega^* : D_T\mathcal{F}_\omega(x) \leq (1-\beta)D_T\mathcal{F}_\omega^*\right\} , \tag{4.3}$$

where $\beta \in (0, 1)$ is chosen in such a way that $|\omega^\beta| \approx \pi\delta^2/4$ (and $|\omega^\beta| \leq \pi\delta^2/4$) is satisfied, where δ represents the thickness of the initial damage. The steps of the new algorithm are detailed below in the form of a pseudo-code, see Algorithm 1.

Note that the line 13 in the Algorithm 1 represents the crack propagation process. For more details concerning the Algorithm 1, see [19].

5. Numerical experiments

In all examples, the reference domain Ω represents one block of the reservoir which contains a single geological fracture. In particular, the domain Ω is given by a square with dimension (5×5) m² as shown in Fig. 4. The preexisting geological fracture is represented by an initial damage with length h and width δ. The region to be fractured is identified by the distribution of elastic material and the compliant material is used to represent the geological fracture. Homogeneous Dirichlet boundary conditions are considered in all sides of the domain, except in the last example concerning in-situ stress. The structure is assumed to be under plane strain assumption and the total intensity of the prescribed pressure $\bar{p}$ on Γ_D is divided into $N = 200$ uniform increments. Finally, linear triangular finite elements are used to discretize the hydro-mechanical coupled system.

5.1. Benchmark example

In this first example, the geological fracture is located at the center of the bottom side immediately above the pressurization well. The modulus of elasticity E, the Poisson ratio ν, the permeability of the medium k and the

---

**Algorithm 1:** Damage evolution algorithm.

    Input : Ω, ω, δ, N, $\overline{p}_0$, $\Delta\overline{p}_i$
    Output: Optimal topology ω^*

1 **for** $i = 1 : N$ **do**
2   solve the pressure problem (2.5);
3   solve the coupled elasticity system (2.4);
4   solve the adjoint state (2.15);
5   evaluate the topological derivative $D_T\mathcal{F}_\omega$ according to (3.89);
6   compute the threshold ω^* from (4.1);
7   **while** $|\omega^*| \geq \pi\delta^2/4$ **do**
8   intensify the mesh at the crack tip;
9   solve the pressure problem and the coupled elasticity system;
10   solve the adjoint state and evaluate the topological derivative $D_T\mathcal{F}_\omega$;
11   compute the threshold ω^* from (4.1);
12   compute the threshold ω^β from (4.3);
13   nucleate a new inclusion ω^β inside ω^*;
14   update the damaged region: $\omega \leftarrow \omega \cup \omega^\beta$;
15   solve the pressure, elasticity and adjoint problems and evaluate $D_T\mathcal{F}_\omega$;
16   evaluate the shape functional $\mathcal{F}_\omega$ from (2.2);
17   if the shape functional increases, then break;
18   else compute the threshold ω^*;
19   **end while**
20 **end for**
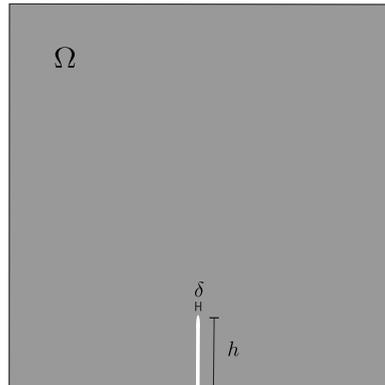
Fig. 4. Benchmark example: One block of the reservoir containing a single geological fracture.

Biot's coefficients α^m at the matrix and α^f at the fracture corresponds to the values from [5]. All data of the present example are summarized in Table 1, where the parameter l represents the diameter of the inclusion.

The first observed critical pressure was $p_c^1 = 3, 68$ MPa at pseudo time-step $i = 184$. The material distribution after the damage evolution induced by this first critical pressure is presented in Fig. 5(a). Fig. 5(b) shows the history of the shape functional $\mathcal{F}_\omega$ from (2.2) during the optimization process described by the internal loop of Algorithm 1. Note that the model dissipates energy in all iterations. After then, three new critical pressures have been detected, namely, $p_c^2 = 3, 84$ MPa at pseudo time-step $i = 192$, $p_c^3 = 3, 92$ MPa at pseudo time-step $i = 196$ and $p_c^4 = 3, 96$ MPa at pseudo time-step $i = 198$. The observation of distinct critical pressures is due to the pressure drop while the geological fracture grows. Since the damage evolution associated with each new critical pressure is small with respect to the propagation related with the first critical pressure, only the final result is shown in Fig. 6.

Table 1
Benchmark example: Parameters.

Parameter	Value	Parameter	Value
h	1, 0 m	E	17.000 MPa
δ	0, 025 m	ρ_0	10^{-6}
l	$(2/3)\delta$	ν	0, 2
$\overline{p}$	4, 0 MPa	κ_s	590, 0 J/m
k	1, 0 mD	α^m	0, 1
γ^f	10^3	α^f	1, 0

(a)   (b)
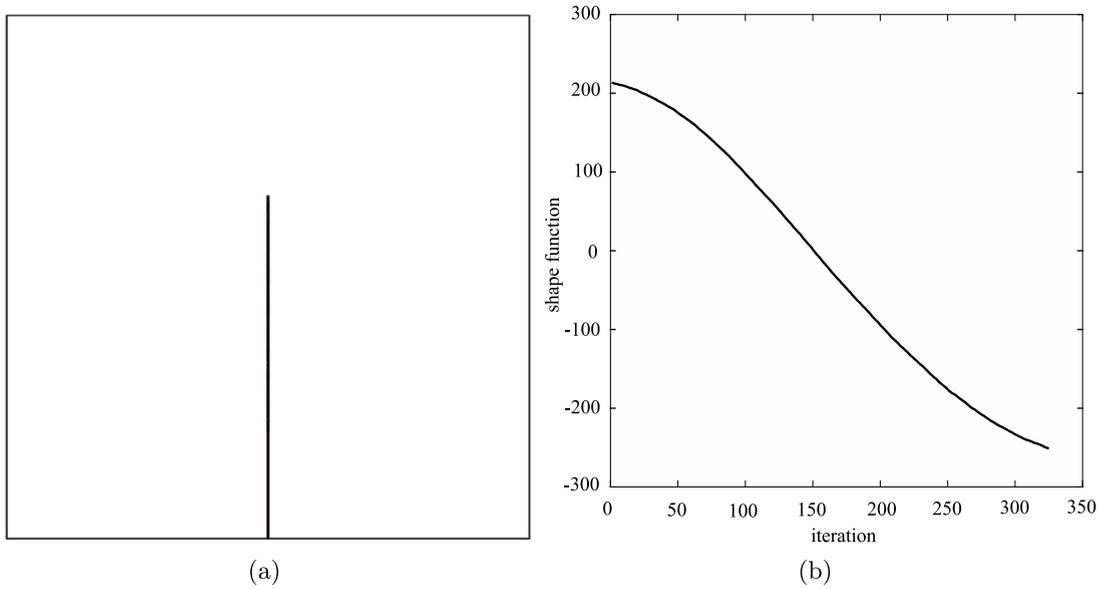
Fig. 5. Benchmark example: Results for $p_c^1 = 3, 68$ MPa at pseudo time-step $i = 184$, (a) obtained damage distribution and (b) history of the shape functional $\mathcal{F}_\omega$ from (2.2) during the optimization process described by the internal loop of Algorithm 1.
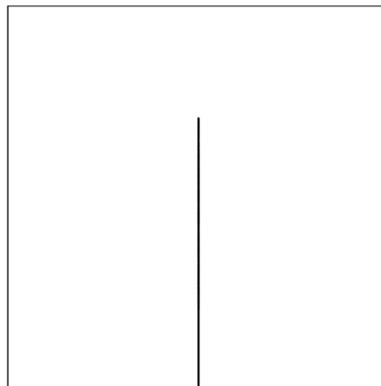
Fig. 6. Benchmark example: Damage distribution for $p_c^4 = 3,96$ MPa at pseudo time-step $i = 198$.

The pressure distribution at the precise moment before the first propagation and at the end of the entirely process can be observed in Figs. 7(a) and 7(b), respectively.
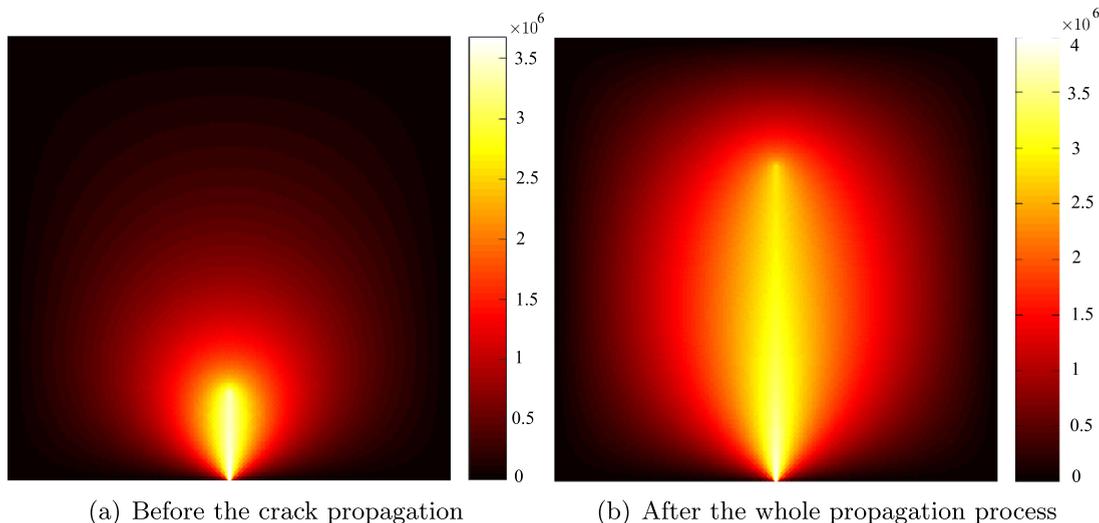
(a) Before the crack propagation

(b) After the whole propagation process

Fig. 7. Benchmark example: Pressure distribution.

Table 2
Stratified block: Parameters.

Parameter	Value	Parameter	Value
h	1,0 m	E_1	17.000 MPa
δ	0,025 m	ρ_0	10^{-6}
l	$(2/3)\delta$	ν	0,2
$\bar{p}$	8,0 MPa	κ_s	590,0 J/m
k_1	1,0 mD	α^m	0,1
γ^f	10^3	α^f	1,0

5.2. Stratified block

In this next example, we consider a stratified block composed by two layers with different permeability and modulus of elasticity, namely, $k_1 = 1$ mD and $k_2 = 0,5 \times k_1$ and $E_1 = 17$ GPa and $E_2 = 2 \times E_1$. Two cases are considered, which are referred to as Case 1 and Case 2. The different cases treated in this example differ from each other by the spatial distribution of the material properties as indicated in Figs. 8(a) and 8(b), representing Case 1 and Case 2, respectively. The parameters used in this example are summarized in Table 2. In Case 1, twenty one distinct critical pressures have been detected, the first one was $p_c^1 = 3,80$ MPa at pseudo time-step $i = 190$ and the last one $p_c^{21} = 5,56$ MPa at pseudo time-step $i = 278$. In Case 2, twelve critical pressures were observed, with $p_c^1 = 6,36$ MPa at pseudo time-step $i = 318$ and $p_c^{12} = 7,88$ MPa at pseudo time-step $i = 394$. Once again, the observation of different critical pressures is due to the pressure drop while the geological fracture grows. The damage distributions at the end of the optimization process are presented in Fig. 9. Combinations such as (E_1, k_2) and (E_2, k_1) produce the similar results.

5.3. Heterogeneous medium

In this example, a heterogeneous medium is considered again. However, in this case the permeability k and the Young's modulus E are corrupt with White Gaussian Noise (WGN) of zero mean and standard deviation τ. Therefore, k and E are replaced by $k_\tau = k(1 - \tau_p s)$ and $E_\tau = E(1 + \tau_e s)$, where $s : \Omega \to \mathbb{R}$ is a function assuming random values in the interval $(0, 1)$ and $\tau_p = 0,5$ and $\tau_e = 2,0$ corresponds to the noise levels. The parameters are presented in Table 3. Figs. 10(a) and 10(b) show the corrupted Young's modulus $E_\tau(x)$ and the corrupted permeability $k_\tau(x)$, respectively. The resulting damage evolution associated with each detected critical
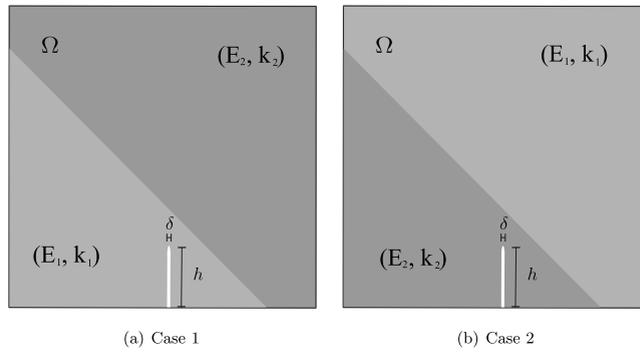
(a) Case 1   (b) Case 2

Fig. 8. Stratified block with different material distribution.

(a) Case 1: $p_c^1 = 3,80$ MPa at $i = 190$ (b) Case 1: $p_c^{21} = 5,56$ MPa at $i = 278$

(c) Case 2: $p_c^1 = 6,63$ MPa at $i = 318$ (d) Case 2: $p_c^{12} = 7,88$ MPa at $i = 394$
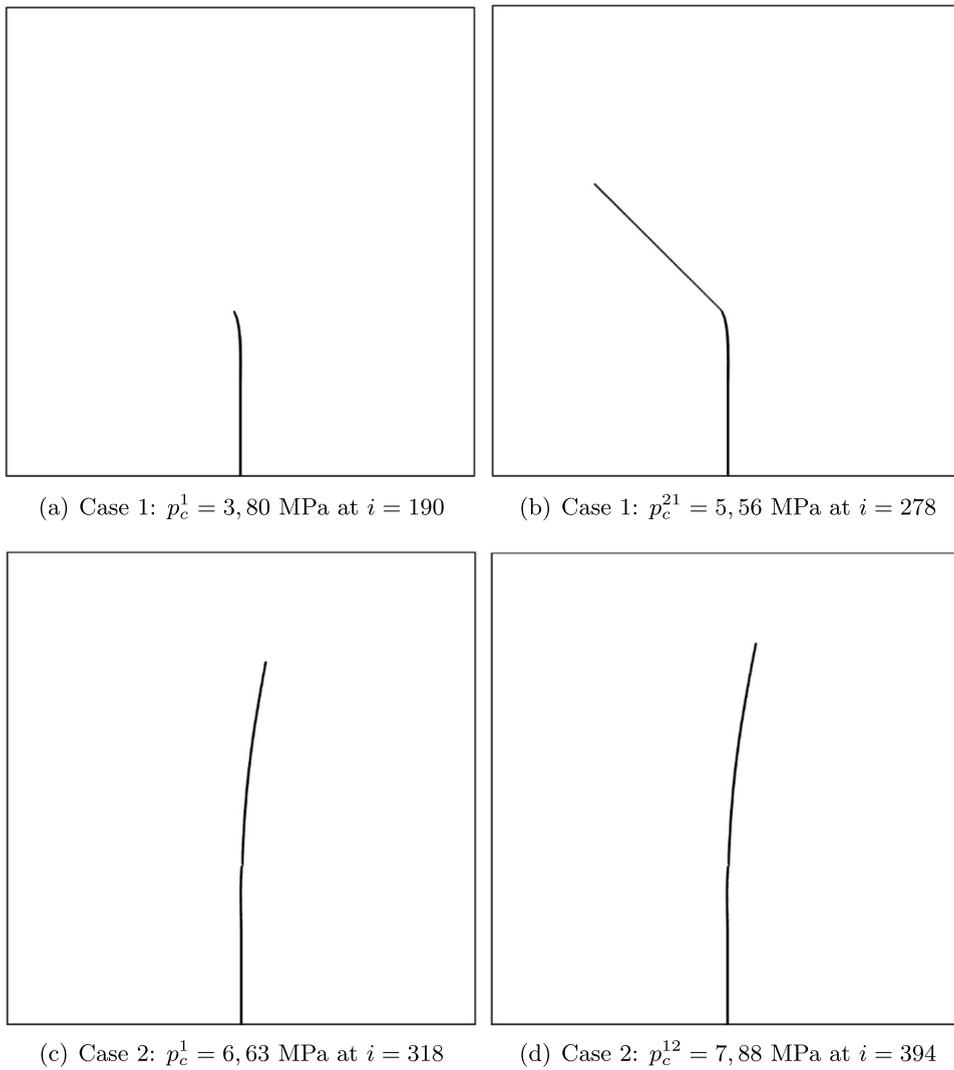
Fig. 9. Stratified block: Final results.

(a) Corrupted Young's modulus   (b) Corrupted permeability
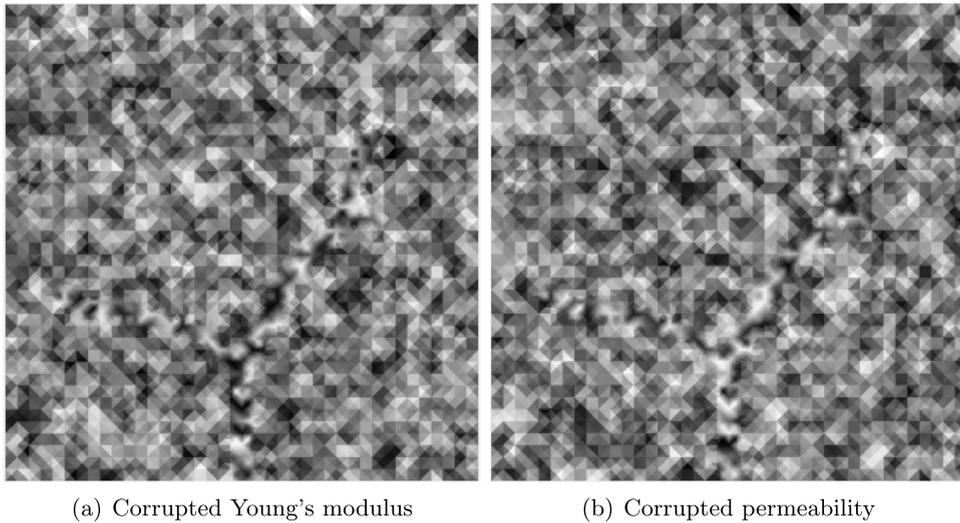
Fig. 10. Heterogeneous medium.

Table 3
Heterogeneous medium: Parameters.

Parameter	Value	Parameter	Value
h	1,0 m	E	17.000 MPa
δ	0,0625 m	ρ_0	10^{-6}
l	$(2/3)\delta$	ν	0,2
$\overline{p}$	8,0 MPa	κ_s	590,0 J/m
k	1,0 mD	α^m	0,1
γ^f	10^3	α^f	1,0

Table 4
Block subject to in-situ stresses effects: Parameters.

Parameter	Value	Parameter	Value
h	1,0 m	E	17.000 MPa
δ	0,0625 m	ρ_0	10^{-6}
l	$(2/3)\delta$	ν	0,2
$\overline{p}$	4,0 MPa	κ_s	190.000 J/m
k	1,0 mD	α^m	0,1
γ^f	10^3	α^f	1,0

pressure is presented in Fig. 11. Note that, due to the heterogeneity of the medium, we can observe kinking and bifurcations phenomena, which is expected from the physical point of view.

5.4. Block subject to in-situ stresses effects

In this last example, we consider that the reservoir is subject to a uniaxial loading which induces a traction tension $\sigma_H = 50$ MPa acting horizontally, representing the in-situ stress. The preexisting geological fracture is located at the center of the block forming an angle of $30°$ with respect to the horizontal axis, as shown in Fig. 12(a). The parameters used in this example are presented in Table 4. The related critical pressure was $p_c = 1,08$ MPa at $i = 54$. The result can be observed in Fig. 12(b). Note that, instead propagates straight following the main axis of the initial fault, the crack reorients itself along the vertical direction, forming two opposite kinks at the crack tips [25].
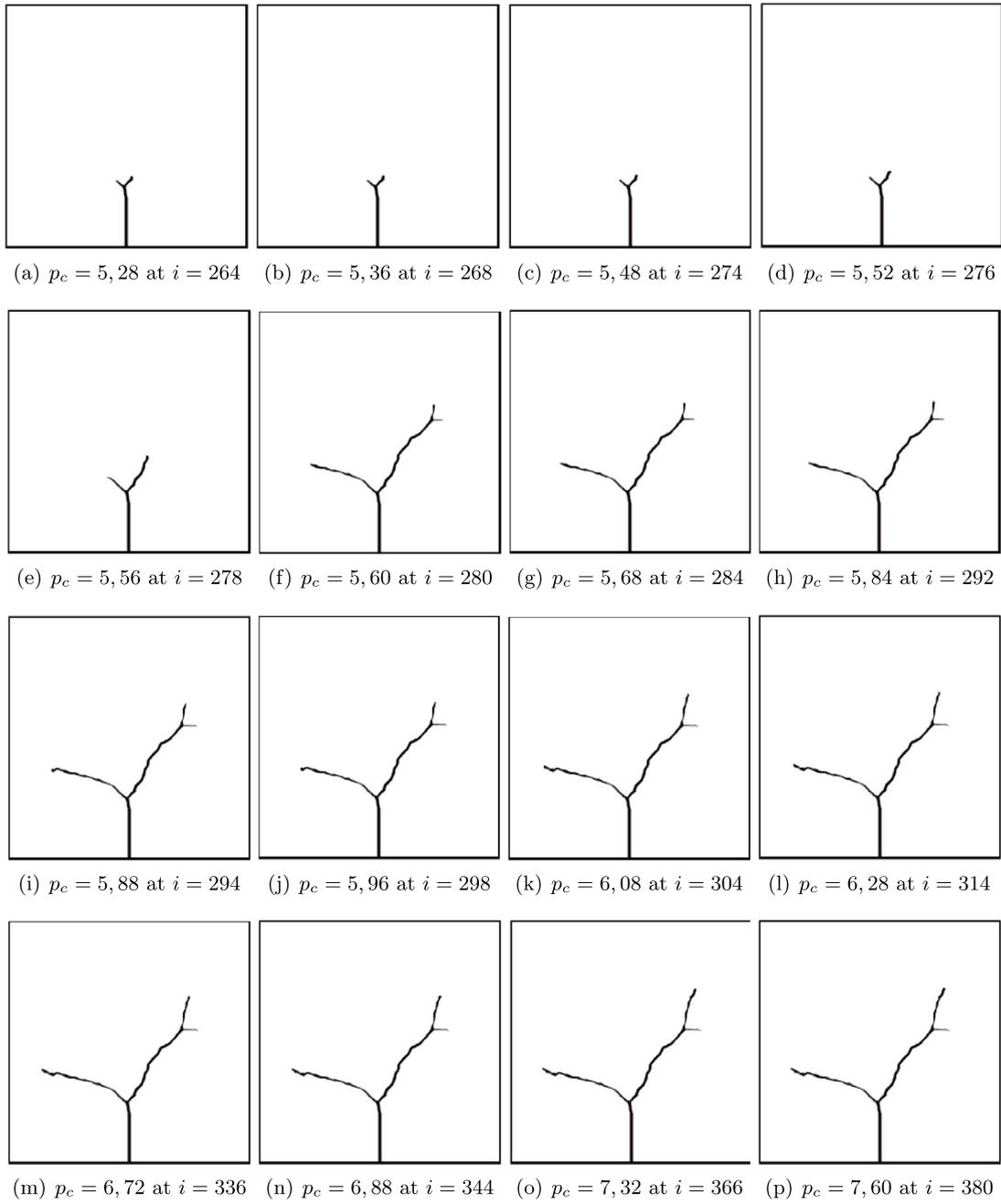
(a) $p_c = 5,28$ at $i = 264$ (b) $p_c = 5,36$ at $i = 268$ (c) $p_c = 5,48$ at $i = 274$ (d) $p_c = 5,52$ at $i = 276$

(e) $p_c = 5,56$ at $i = 278$ (f) $p_c = 5,60$ at $i = 280$ (g) $p_c = 5,68$ at $i = 284$ (h) $p_c = 5,84$ at $i = 292$

(i) $p_c = 5,88$ at $i = 294$ (j) $p_c = 5,96$ at $i = 298$ (k) $p_c = 6,08$ at $i = 304$ (l) $p_c = 6,28$ at $i = 314$

(m) $p_c = 6,72$ at $i = 336$ (n) $p_c = 6,88$ at $i = 344$ (o) $p_c = 7,32$ at $i = 366$ (p) $p_c = 7,60$ at $i = 380$

Fig. 11. Heterogeneous medium: damage evolution for each obtained critical pressure in MPa.

6. Towards 3D fracking

In this section we present the topological derivative associated with the hydro-mechanical model of Section 2 in three spatial dimensions. The derivations follow the same steps as presented in Section 3. In particular, the topological derivative of the energy shape functional, written in terms of the Young modulus and Poisson ratio, is
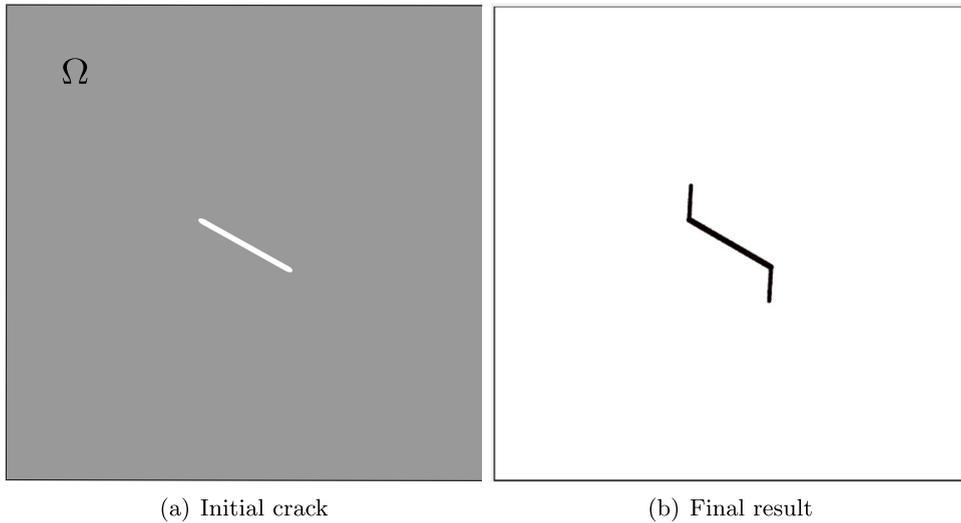
(a) Initial crack (b) Final result

Fig. 12. Block subject to in-situ stresses effects.

given by

$$D_T \mathcal{J}(x) = \mathbb{P}_\gamma \sigma(u)(x) \cdot (\nabla u)^s(x) + 3a(1 - \gamma^\alpha)\alpha p(x)\,\mathrm{div}(u)(x)$$
$$-\frac{3}{2}\frac{(3a-1)(1-2\nu)}{\rho \mathrm{E}(1-\gamma)}(1-\gamma^\alpha)^2\alpha^2 p(x)^2 - 3\frac{1-\gamma^f}{2+\gamma^f}k\nabla p(x)\cdot\nabla q(x)\,, \qquad (6.1)$$

where the polarization tensor $\mathbb{P}_\gamma$ is now defined as

$$\mathbb{P}_\gamma = -\frac{1-\gamma}{2}\left(3b\mathbb{I} + (a-b)\,\mathrm{I}\otimes\mathrm{I}\right)\,, \qquad (6.2)$$

with the coefficients a and b redefined as follows

$$a = \frac{(1-\nu)}{3(1-\nu)-(1+\nu)(1-\gamma)} \quad \text{and} \quad b = \frac{5(1-\nu)}{15(1-\nu)-(8-10\nu)(1-\gamma)}\,. \qquad (6.3)$$

The displacement u, the pressure p and the adjoint pressure q are solutions of the three dimensional counter-parts of the variational problems (2.4), (2.5) and (2.15), respectively. We note however that in order to apply the result (6.1) in the fracking modeling context, Algorithm 1 has to be adapted to the three dimensional case accordingly, which seems to be not straightforward, requiring further developments.

7. Conclusion

The first challenge of this study was to show that a simple model of hydro-mechanical crack propagation in permeable rocks was possible. Simple means (i) based on the minimization of an energy shape functional; (ii) governed by the computation of a single field, the topological derivative, able to determine nucleation, advance, bifurcation of multiple cracks; with a minimal number of user-defined algorithmic parameters. This aim was achieved, and the simulations we made showed good to very good agreement with known benchmark examples obtained by other methods. We emphasize also that an extremely simple numerical method, namely triangular finite elements was used to compute all mechanical fields including the crack aperture. In this work the model was limited to two-dimensional domains but the three dimensional case is already a work in progress, as shown in Section 6. Transient effects are also a matter of future research.

References

[1] T.D. Cao, E. Milanese, E.W. Remij, P. Rizzato, J.J.C. Remmers, L. Simoni, J.M. Huyghe, F. Hussain, B.A. Schrefler, Interaction between crack tip advancement and fluid flow in fracturing saturated porous media, Mech. Res. Commun. 80 (2017) 24–37.

[2] Y. Feng, K.E. Gray, Parameters controlling pressure and fracture behaviors in field injectivity tests: A numerical investigation using coupled flow and geomechanics model, Comput. Geotech. 87 (2017) 49–61.

[3] J. Kim, G.J. Moridis, Numerical analysis of fracture propagation during hydraulic fracturing operations in shale gas systems, Int. J. Rock Mech. Min. Sci. 76 (2015) 127–137.

[4] E. Milanese, O. Yilmaz, J.F. Molinari, B.A. Schrefler, Avalanches in dry and saturated disordered media at fracture, Phys. Rev. E 93 (2016) 043002.

[5] S. Salimzadeh, A. Paluszny, R.W. Zimmerman, Three-dimensional poroelastic effects during hydraulic fracturing in permeable rocks, Int. J. Solids Struct. 108 (2017) 153–163.

[6] S. Secchi, B.A. Schrefler, A method for 3-d hydraulic fracturing simulation, Int. J. Fract. 178 (1) (2012) 245–258.

[7] M.Y. Soliman, M. Wigwe, A. Alzahabi, E. Pirayesh, N. Stegent, Analysis of fracturing pressure data in heterogeneous shale formations, Hydraul. Fract. J. 1 (2) (2014) 8–12.

[8] G.Q. Zhang, M. Chen, Dynamic fracture propagation in hydraulic re-fracturing, J. Pet. Sci. Eng. 70 (2010) 266–272.

[9] C. Chukwudozie, B. Bourdin, K. Yoshioka, A variational phase-field model for hydraulic fracturing in porous media, Comput. Methods Appl. Mech. Engrg. 347 (2019) 957–982.

[10] G. Francfort, J.J. Marigo, Revisiting brittle fracture as an energy minimization problem, J. Mech. Phys. Solids 46 (8) (1998) 1319–1342.

[11] G.A. Francfort, J.J. Marigo, Stable damage evolution in a brittle continuous medium, Eur. J. Mech. A/Solids 12 (2) (1993) 149–189.

[12] A. Mikelic, M.F. Wheeler, T. Wick, A phase-field method for propagating fluid-filled fractures coupled to a surrounding porous medium, Multiscale Model. Simul.: A SIAM Interdiscip. J. Soc. Ind. Appl. Math. 13 (2015) 367–398.

[13] A. Mikelic, M.F. Wheeler, T. Wick, Phase-field modeling of a fluid-driven fracture in a poroelastic medium, Comput. Geosci. 19 (2015) 1171–1195.

[14] G. Allaire, F. Jouve, N. Van Goethem, A level set method for the numerical simulation of damage evolution, in: ICIAM Proceedings, Zürich, Switzerland, 2007.

[15] J. Céa, S. Garreau, P. Guillaume, M. Masmoudi, The shape and topological optimizations connection, Comput. Methods Appl. Mech. Engrg. 188 (4) (2000) 713–726.

[16] J. Sokołowski, A. Żochowski, On the topological derivative in shape optimization, SIAM J. Control Optim. 37 (4) (1999) 1251–1272.

[17] N. Van Goethem, A.A. Novotny, Crack nucleation sensitivity analysis, Math. Methods Appl. Sci. 33 (16) (2010) 1978–1994.

[18] M. Xavier, E.A. Fancello, J.M.C. Farias, N. Van Goethem, A.A. Novotny, Topological derivative-based fracture modelling in brittle materials: A phenomenological approach, Eng. Fract. Mech. 179 (2017) 13–27.

[19] M. Xavier, A.A. Novotny, N. Van Goethem, A simplified model of fracking based on the topological derivative concept, Int. J. Solids Struct. 139–140 (2018) 211–223.

[20] M. Caroccia, N. Van Goethem, Damage-driven fracture with low-order potentials: asymptotic behavior, existence and applications, ESAIM: M2AN 53 (4) (2019) 1305–1350.

[21] M.A. Biot, General theory of three-dimensional consolidation, J. Appl. Phys. 12 (2) (1941) 155–164.

[22] A.A. Novotny, J. Sokołowski, Topological derivatives in shape optimization, in: Interaction of Mechanics and Mathematics, Springer-Verlag, Berlin, Heidelberg, 2013, p. 324.

[23] J.D. Eshelby, The determination of the elastic field of an ellipsoidal inclusion, and related problems, Proc. R. Soc. A 241 (1957) 376–396.

[24] J.D. Eshelby, The elastic field outside an ellipsoidal inclusion, and related problems, Proc. R. Soc. A 252 (1959) 561–569.

[25] C. Chukwudozie, B. Bourdin, K. Yoshioka, A variational approach to the modeling and numerical simulation of hydraulic fracturing under in-situ stresses, in: Proceedings of the 38th Workshop on Geothermal Reservoir Engineering, 2013.